Exergy Analysis of Steam Methane Reforming Process in Computational Fluid Dynamics (CFD) Environment

By

Zia ur Rahman

School of Chemical and Materials Engineering

National University of Sciences and Technology

2019

Exergy Analysis of Steam Methane Reforming Process in Computational Fluid Dynamics (CFD) Environment

Zia ur Rahman

2015-MS CHE-03-00000119719

This work is submitted as a MS thesis in partial fulfillment of the requirement for the degree of

MS in Chemical Engineering

Supervisor Name: Dr. Iftikhar Ahmad

School of Chemical and Materials Engineering (SCME)

National University of Sciences and Technology (NUST)

H-12 Islamabad, Pakistan

April, 2019

Dedication

To my Parents and Siblings

Abstract

Steam methane reforming (SMR) is a dominant technology for hydrogen production. For the highly energy-efficient operation, robust energy analysis is crucial. In particular, exergy analysis has received the attention of researchers due to its advantage over the conventional energy analysis. In this work, an exergy analysis based on the computational fluid dynamics (CFD)-based method was applied to a monolith microreactor of SMR. Initially, a CFD model of SMR was developed using literature data. Then, the design and operating conditions of the microreactor were optimized based on the developed CFD model to achieve higher conversion efficiency and shorter length. Exergy analysis of the optimized microreactor was performed using the custom field function (CFF) integrated with the CFD environment. The optimized catalytic monolith microreactor of SMR achieved higher conversion efficiency at a smaller consumption of energy, catalyst, and material of construction than the reactor reported in the literature. The exergy analysis algorithm helped in evaluating length-wise profiles of all three types of exergy, namely, physical exergy, chemical exergy, and mixing exergy, in the microreactor.

Keywords: steam methane reforming; computational fluid dynamics; monolith reactor; physical exergy; chemical exergy; CHEMKIN; rhodium catalyst; simple algorithm

Acknowledgments

First of all, I would like to thank Almighty Allah who showered his blessings on me and helped me to complete this work.

This dissertation would not have been possible without the guidance and the help of several individuals who in one way or another contributed, and extended their valuable assistance in the preparation and completion of this study.

I would also like to express my sincere gratitude to my supervisor **Dr. Iftikhar Ahmad** for his guidance, patience, and motivation throughout this research work. His exemplary guidance, steadfast encouragement, perceptive criticism, and valuable suggestions were of immense help throughout my project work and shall carry me a long way in the journey of life on which I am about to embark.

I would like to thank my guidance and examination committee members **Dr. Muhammad Ahsan**, and **Dr. Muhammad Taqi Mehran** for their valuable guidance.

Last but not least my appreciation also goes to my family and friends for their encouragement, love, and support throughout my life.

Abbreviations

Computational fluid dynamic	CFD
Steam methane reforming	SMR
Water gas shift reaction	WGS
Pressure swing adsorption	PSA
Steam to Carbon ration	S/C
Semi-implicit method for pressure linked equation	SIMPLE
Physical exergy	E^{ph}
Chemical exergy	E^{ch}
Mixing exergy	E^{mix}
Mass flux	J_i
Molar Gibbs Function	$\bar{G}_i$
Gibbs function of formation	G_f^0
Stoichiometric coefficient	v_i
Ideal Gas Constant	R
Diffusion coefficient	D_i
Mass fraction	Y_i
Pre Exponential Factor	A_k
Activation Energy	E_{a_r}
Forward rate coefficient	$k_{f,r}$

TABLE OF CONTENTS

List of Figures

List of Tables

Chapter 1

Introduction

The need for hydrogen production is growing rapidly due to its immense importance in the petroleum and chemical industry as shown in Figure 1.1. Hydrogen is mainly used for the up-gradation of fossil fuels and ammonia production. The use of hydrogen as a fuel has also recently increased due to its high heating value and less-polluting nature [1]. It is used in different other applications such as fuel cells, metal production, and power generation [2].

The steam reforming of methane gas is the abundantly used method for the production of hydrogen. Saeidi et al. [3] estimated that 48% of all hydrogen production came from the steam reforming of methane as shown in Figure 1.2. However, steam methane reforming (SMR) has several limitations, such as heat transfer limitation, mass transfer limitation, and catalyst deactivation [1]. To cope with these limitations, conventional SMR is being transformed into micro-reforming technology, which overcomes the heat transfer limitation and enhances the mass transfer; as a result, micro-reforming technology improves the conversion efficiency [4]. The intensified form of SMR (i.e., micro size plant) increases profit margins above 70% for the same capacity of H2 production [1].

Since SMR is endothermic and energy intensive, a robust energy analysis of the micro-scale SMR is also needed [5]. The concept of exergy has attracted the attention of researchers and process designers because of its capability to evaluate the true thermodynamic potential of a process. Exergy analysis helps in the identification of the locations, causes, and quantification of irreversibility and wastages in a system [6].

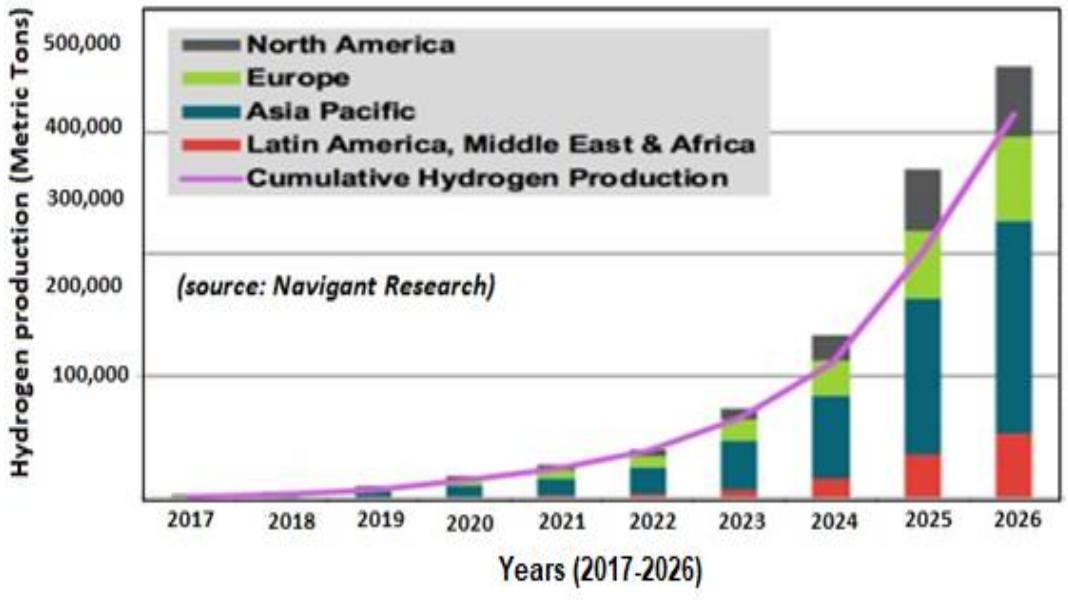

Figure 1.1: Annual cumulative hydrogen production by region

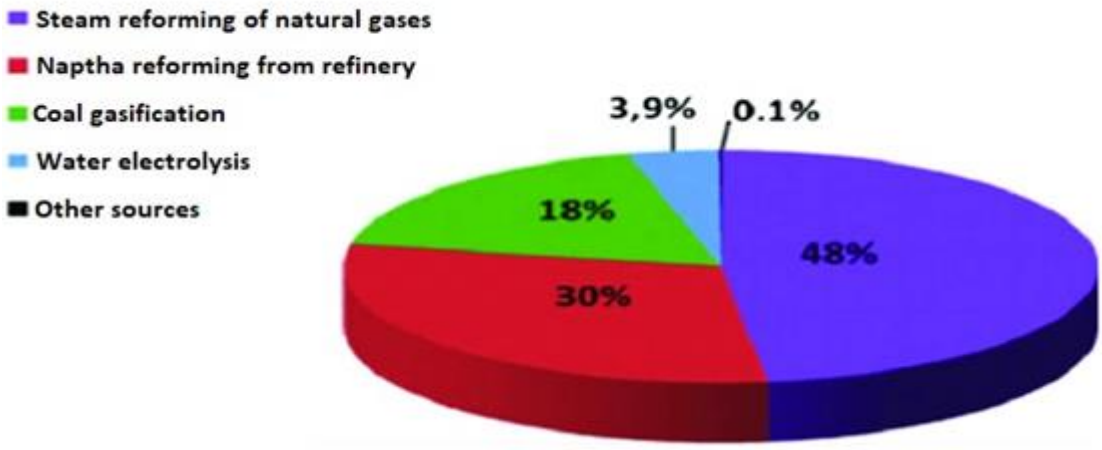

Figure 1.2: Percentages of different sources of hydrogen production

In this work, exergy analysis of a monolith microreactor of SMR was performed by using a computational fluid dynamics (CFD) model. Initially, the CFD model was developed using literature data. The monolith catalyst bed was used by considering its large surface area, low-pressure drop, high durability, and high mechanical strength. Monolith catalyst structure consists of a number of tubes in a single unit. A cross-sectional area of the single tube is shown in Figure 1.3 which consist of catalytic material wash coat at the inner side of the tube wall and exhaust gas channel is present in the middle of the tube.

The surface-based approach was used for modeling reaction rates. To incorporate reaction kinetics, the CHEMKIN mechanism was used. Size of the reactor and operation conditions were optimized to realize higher conversion efficiency and smaller capital and operational costs. To analyze true thermodynamic efficiency, its exergy analysis was performed by developing a custom field function (CFF)-based algorithm. The exergy analysis algorithm helps in evaluating length-wise profiles of all three types of exergy, namely, physical exergy, chemical exergy, and mixing exergy, in the microreactor.

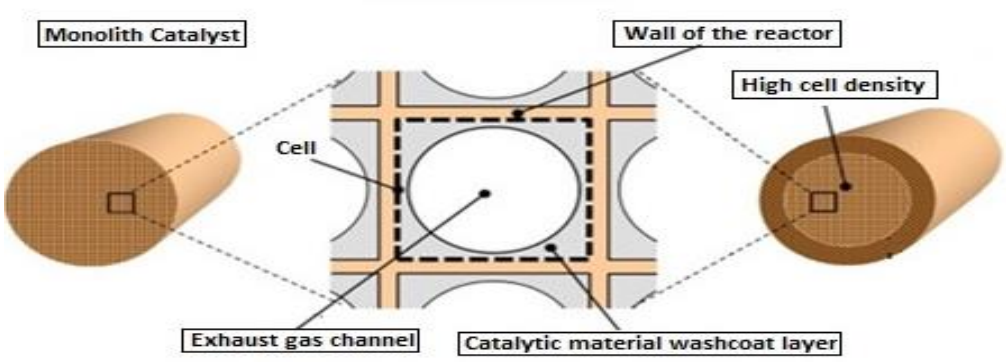

Figure 1.3: Monolith catalyst structure

1.2 Thesis Outline

The introduction are discussed in Chapter 1. Basic theoretical concepts, governing equations, exergy, and steam methane reforming processes are evaluated in Chapter 2. Literature survey and objectives is illustrated in Chapter 3. The procedure for CFD based model development is discussed in Chapter 4. Chapter 5 illustrates the development of exergy quantification tool, geometry preparation, and simulation. Results, conclusions, and suggestions for future are described in Chapter 6.

Chapter 2

Theoretical Background

2.1 Steam Methane Reforming Process

Hydrogen is produced mainly in four steps, i.e., natural gas pretreatment, reforming process, shift reaction, and purification, as shown in Figure 2.1 [7].

In the pretreatment step, the unwanted components present in the feed gas (methane) are separated to prevent the catalyst from poisoning. The zinc oxide bed captures the sulfur-containing compounds such as hydrogen sulfide and leaves the gas with sulfur impurities smaller than 1 ppm [8].

In the reforming process, the methane–steam mixture is converted with the help of catalyst into H_2, CO, and CO_2 in the reformer according to the following reactions.

$$CH_4 + H_2O \leftrightarrow 3H_2 + CO \qquad \Delta H^o 298 = +206 \text{ kJ/mole} \qquad (2.1)$$

$$CH_4 + H_2O \leftrightarrow 4H_2 + CO_2 \qquad \Delta H^o 298 = +165 \text{ kJ/mole} \qquad (2.2)$$

The reforming reaction is highly endothermic, therefore heat is supplied through the external burners to maintain the temperature and pressure at 1100-1500 ^oC and 1-5 atm, respectively. The side burners are operated to heat the furnaces which provide heat to the tubes of the reformer through forced convection and radiation. The reformer furnace normally consists of a number of tubes, i.e., in the range of 40-400, calculated according to the plant design capacity. Different structures and classifications of the monolith catalyst support channels are shown in Figure 2.2 [4].

The third step is the gas shift reaction. The syngas exiting the reformer takes part in a water–gas shift (WGS) reaction. It transform CO and H_2O in the product gas to H_2 and CO_2 by the following reaction.

$$CO + H_2O \leftrightarrow H_2 + CO_2 \qquad \Delta H^o 298 = -41 \text{ kJ/mole} \qquad (2.3)$$

In the fourth step, which is the purification of hydrogen stream, CO_2 is removed through chemical absorption and unreacted methane is separated by pressure swing adsorption (PSA).

In this work, a two-dimensional CFD model of a single micro reformer tube of monolith catalytic reactor is redesigned [9]. The single reformer tube is shown in Figure 2.3, and the model parameters are mentioned in Table 2.1.

The steam and methane mixture with the ratio of three is provided to the reactor. Inlet velocity is maintained at 0.45 m/s and temperature at 800^{o}C. The mole fraction of methane and steam are 0.23 and 0.77, respectively. A heating jacket surrounds the monolithic reactor and provides the heat of reaction to maintain the temperature same i.e., 1477^{o}C at the walls of reactor. The inlet H_2O/CH_4 molar ratio is kept constant at 3 and the operating pressure is atmospheric.

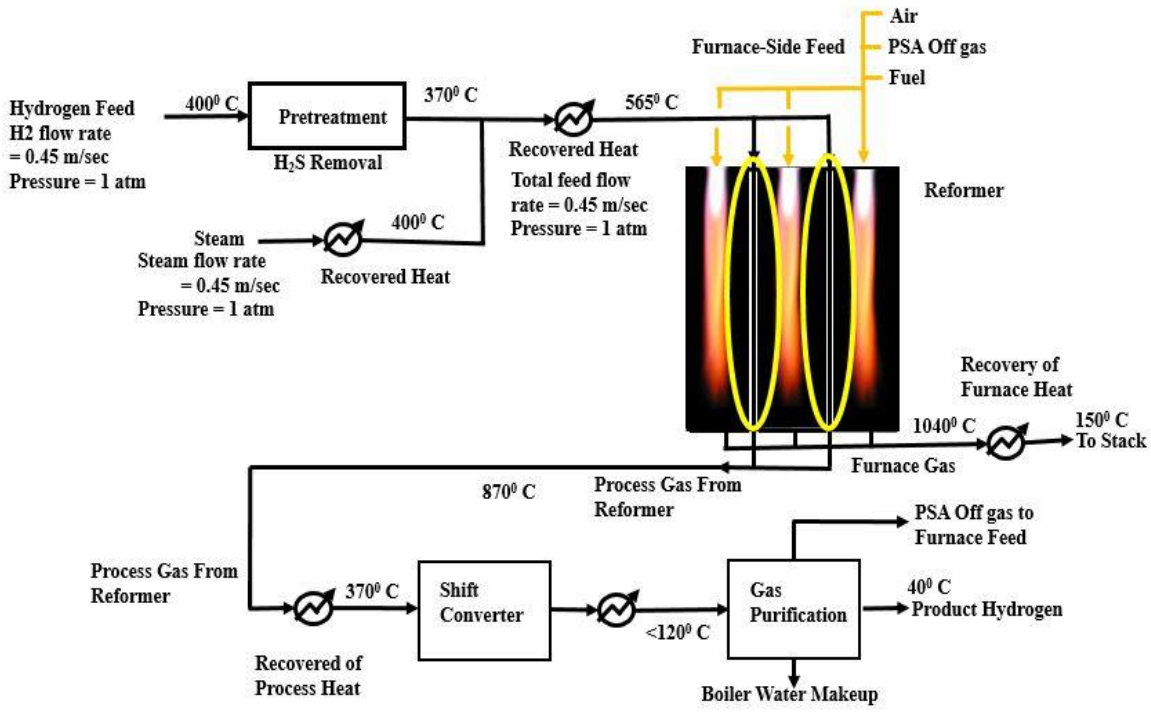

Figure 2.1: Process flow sheet of the SMR process [10]

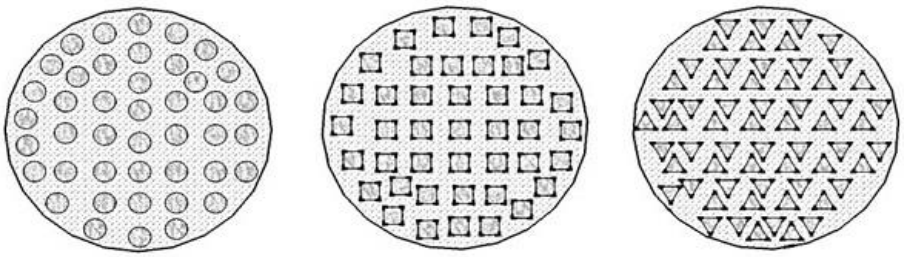

Figure 2.2: Circular, square and trigonal shape arrangement of monolith reactors[4]

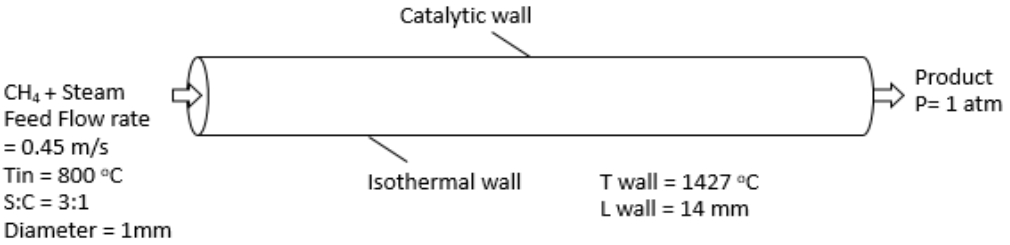

Figure 2.3: A single tube of a monolith catalyst reformer

Table 2.1: Model parameters

Parameters	Symbol	Value
Channel length	L	14mm
Channel diameter	D	1mm
Inlet temperature	T_{in}	800°c
Isothermal wall temperature	T_w	1477°c
Pressure	P	1 atm
The ratio of steam to methane	S/C	3:1
Inlet velocity	V_{in}	0.45m/s
Number of catalyst active site (catalyst density)	Γ	$2.7e^{-9}mol/cm^2$

2.2 Reaction Kinetics of Steam Methane Reforming Process

The heterogeneous reaction mechanism proposed by Karakaya et al. is used for SMR process with rhodium catalyst [11]. It involves 44 elementary reactions as shown in Table 2.2 consists of 6 gaseous and 13 species at the wall surface. The rhodium catalyst is exploited having surface site density Γ_{Rh} = 2.72 × 10^{-9} mole/cm^2. The overall molar rate of creation of *i*-th species through surface reactions is according to the following equation [12] ;

$$\dot{S}\iota = \sum_{n=1}^{n_s} v_{i,n} k_{f,r} \prod_{j=1}^{Ng+Ns} {C_j}^{v'_{j,n}} , \tag{2.4}$$

where $\dot{S}\iota$ is the overall rate expression of *i*-th species for gas-phase or surface phase, n_s is the number of surface elementary reactions, $v_{i,n}$ and $v'_{j,n}$ are the stoichiometric coefficients, and Ng and Ns are the number of gas-phase and surface species, respectively. The concentrations C_j of adsorbed species are given in a mole/m^2.

As binding states of the adsorption of total components changing with the surface coverage, the temperature dependence of the reaction rate coefficients is calculated by employing the modified Arrhenius expression [13].

$$K_{f,r} = A_{kr} T^{\beta_{kr}} exp\left(-\frac{E_{a_r}}{RT}\right) \theta_i^{\mu_{ir}} ex\, p\left[\frac{\varepsilon_{ir}\theta_i}{RT}\right], \tag{2.5}$$

where $k_{f,r}$ is a forward rate coefficient, A_{kr} is the pre-exponential factor, β_{kr} is the temperature exponent, E_{a_r} is the activation energy of the reaction *r*, θ_i is the surface coverage with adsorbed species, and coefficients μ_{ir} and ε_{ir} describe the dependence of the rate coefficients on the surface coverage of i^{th} species.

2.3 Components of Energy

Energy can be subdivided into two main components, one is exergy and the other is anergy. Exergy can produce useful work while the anergy has no ability to do work.

Table 2.2: Elementary reactions and its kinetics for SMR on Rh catalyst [15]

S.No	Reactions	A [mol, cm, s, K]	E_a [KJ/mol]
1.	$H_2+2Rh(s)\rightarrow 2H(s)$		0.0
2.	$2H(s)\rightarrow H_2+2Rh(s)$	3.0×10^{21}	77.8
3.	$O_2+2Rh(s)\rightarrow 2O(s)$		
4.	$2O(s)\rightarrow O_2+2Rh(s)$	1.33×10^{22}	355.2
5.	$CH_4+Rh(s)\rightarrow CH_4(s)$		0.0
6.	$CH_4(s)\rightarrow CH_4+Rh(s)$	2.0×10^{14}	25.1
7.	$H_2O+Rh(s)\rightarrow H_2O(s)$		0.0
8.	$H_2O(s)\rightarrow H_2O+Rh(s)$	6.0×10^{13}	45
9.	$CO_2+Rh(s)\rightarrow CO_2(s)$		0.0
10.	$CO_2(s)\rightarrow CO_2+Rh(s)$	3.0×10^{8}	21.7
11.	$CO+Rh(s)\rightarrow CO(s)$		0.0
12.	$CO(s)\rightarrow CO+Rh(s)$	1.0×10^{13}	133.4
13.	$H(s)+O(s)\rightarrow OH(s)+Rh(s)$	5.0×10^{22}	83.7
14.	$OH(s)+Rh(s)\rightarrow H(s)+O(s)$	3.0×10^{20}	37.7
15.	$H(s)+OH(s)\rightarrow H2O(s)+Rh(s)$	3.0×10^{20}	33.5
16.	$H2O(s)+Rh(s)\rightarrow H(s)+OH(s)$	5.0×10^{22}	106.4
17.	$2OH(s)\rightarrow H_2O(s)+O(s)$	3.0×10^{21}	100.8
18.	$H_2O(s)+O(s)\rightarrow 2OH(s)$	3.0×10^{21}	171.8
19.	$C(s)+O(s)\rightarrow CO(s)+Rh(s)$	5.0×10^{23}	97.9

20.	$CO(s)+Rh(s)\rightarrow C(s)+O(s)$	3.7×10^{21}	169.0
21.	$CO(s)+O(s)\rightarrow CO_2(s)+Rh(s)$	1.0×10^{19}	121.6
22.	$CO_2+Rh(s)\rightarrow CO(s)+O(s)$	5.0×10^{21}	115.3
23.	$CO(s)+H(s)\rightarrow HCO(s)+Rh(s)$	5.0×10^{19}	108.9
24.	$HCO(s)+Rh(s)\rightarrow CO(s)+H(s)$	3.7×10^{21}	0.0
25.	$HCO(s)+Rh(s)\rightarrow CH(s)+O(s)$	8.0×10^{23}	59.5
26.	$CH(s)+O(s)\rightarrow HCO(s)+Rh(s)$	3.7×10^{21}	167.5
27.	$CH_4(s)+Rh(s)\rightarrow CH_3+H(s)$	5.5×10^{20}	61.0
28.	$CH_3+H(s)\rightarrow CH_4(s)+Rh(s)$	3.7×10^{21}	51.0
29.	$CH_3(s)+Rh(s)\rightarrow CH_2(s)+H(s)$	3.7×10^{21}	103.0
30.	$CH_2(s)+H(s)\rightarrow CH_3(s)+Rh(s)$	3.7×10^{21}	44.0
31.	$CH_2(s)+Rh(s)\rightarrow CH(s)+Rh(s)$	3.7×10^{34}	100.0
32.	$CH(s)+Rh(s)\rightarrow CH_2(s)+Rh(s)$	3.7×10^{34}	68.0
33.	$CH(s)+Rh(s)\rightarrow C(s)+H(s)$	3.7×10^{21}	21.0
34.	$C(s)+H(s)\rightarrow CH(s)+Rh(s)$	3.7×10^{21}	172.8
35.	$CH_4(s)+O(s)\rightarrow CH_3(s)+OH(s)$	1.7×10^{24}	80.3
36.	$CH_3(s)+OH(s)\rightarrow CH_4(s)+O(s)$	3.7×10^{21}	24.3
37.	$CH_3(s)+O(s)\rightarrow CH_2(s)+OH(s)$	3.7×10^{24}	120.3
38.	$CH_2(s)+OH(s)\rightarrow CH_3(s)+O(s)$	3.7×10^{21}	15.1
39.	$CH_2(s)+O(s)\rightarrow CH(s)+OH(s)$	3.7×10^{24}	114.5
40.	$CH(s)+OH(s)\rightarrow CH_2(s)+O(s)$	3.7×10^{21}	36.8
41.	$CH(s)+O(s)\rightarrow C(s)+OH(s)$	3.7×10^{21}	30.1

42.	C(s)+OH(s)→ CH(s)+O(s)	3.7×10^{21}	136.0
43.	CO(s)+H(s)→C(s)+OH(s)	3.7×10^{21}	142.0
44.	C(s)+OH(s)→ CO(s)+H(s)	3.7×10^{20}	25.5

The terminology of exergy itself was first reproduce by Zoran in 1956 by combining two Greek words, ex and ergon which means “from work”. Exergy can be stated as;

The paramount of possible work obtainable by bringing a matter from its initial state through a reversible process to a condition of thermodynamic and chemical equilibrium with the reference environment referred as a dead state [16].

Exergy is used as a standard to define the energy quality as it is the only component actually producing work. The energy losses due to the irreversibilities of a real system appear in the entropy form. The relation between exergy and entropy production is shown by the thermodynamics second law. Entropy generation is directly proportional to exergy loss which leads to degradation of exergy in a real process. Thus, the goal of any energy transformation process is to achieve the highest possible exergy out of energy input.

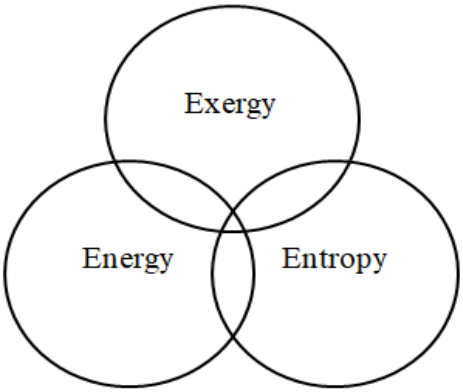

Figure 2.4: Interaction of energy, entropy, and exergy

2.4 Reference Environment

Reference environment can be considered as a large thermodynamic body comprised of various components which are in perfect equilibrium with surrounding. All the components have no difference in pressure, temperature, chemical potential, kinetic

and potential energy. However, defining such an ideal reference environment is challenging. To overcome this difficulty some researchers have suggested a few standard reference environments for exergy analysis. Reference environment used in this work is related to the standard environment stated by Szargut et. al [17]. The model is based on the following components at the standard temperature and pressure i.e., T_0=298.15K and P_0=101.325kPa.

- Atmospheric gaseous components: O_2, N_2, CO_2, H_2O, O_2
- Solid reference substance of the earth crust.
- Sea substances as ionic reference.

Exergy is emitted by a system when it is bring to a state of equilibrium with the environment i.e., at dead state. The dead state requires full thermodynamic equilibrium i.e., mechanical, thermal and chemical equilibrium with the environment.

2.5 Exergy Balances

The Exergy study is rely on the first and second law of thermodynamics. The first law of thermodynamics portrays that energy can never be vanished, on the other hand the second law of thermodynamics states that heat energy cannot be fully brought into service when it is involved with the real system. The wasted energy appears in the form of entropy due to the irreversibilities of the process system. The energy, exergy and entropy relation is shown in Figure 2.5.

The energy flowing in and out are equal in amount, as stated by the first law of thermodynamics; on the other hand, the quantity of entropy moving out is larger than the moving in according to the law of entropy increase. The quantity of exergy moving out is lesser than the moving in. This is due to a portion of exergy is lost within the system due to irreversibilities which appear in the form of entropy.

Mathematical model of exergy is given by the following equation [18].

$$E_{ex(Tot)} = \Delta K.E + \Delta P.E + (h - h_0) - T(S - S_o) + E_{ex(chem)} \quad (2.7)$$

$\Delta E + \Delta H$ = Work ….. 1st law of thermodynamics.

$\Delta S = S_{gen}$ ….. 2^{nd} law of thermodynamics.

The first three terms on the right-hand side of the equation 2.7 are the portion represented by the first law of thermodynamics while the fourth term is the portion represented by the second law of thermodynamics. The exergy equation integrates both the first and second law of thermodynamics to find the maximum amount of work that we can obtain from a system.

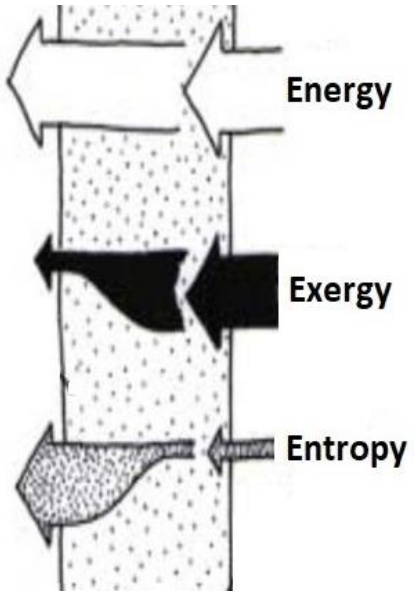

Figure 2.5: Inflow and outflow of energy, exergy, and entropy through a system

2.6 Components of Exergy

Conventionally, the total stream exergy is distributed into three parts: physical exergy, chemical exergy, and mixing exergy. A general expression of exergy is given by the following equation:

$$E = E^{ph} + E^{ch} + E^{mix} \quad (2.8)$$

where E represents total molar exergy of a stream, E^{ph} is the molar physical exergy, E^{ch} is the molar chemical exergy, and E^{mix} is the molar mixture exergy [16].

The paramount of possible work obtainable by bringing a matter from its initial state through a reversible process to a condition of thermodynamic and chemical equilibrium with the reference environment referred to as a dead state

Physical exergy represents the thermo-mechanical portion of the total exergy stream. It is paramount of possible work obtainable by bringing a matter from its initial states (*T, P*) through a reversible process to a condition of thermodynamics and chemical equilibrium with the dead state reference environment (T_o, P_o).

On a molar basis, physical exergy is given by

$$E^{\mathrm{ph}} = \mathrm{R}T_o \sum_{\mathrm{i}=1}^{\mathrm{n}} ln\frac{p_i}{p_o} + \sum_{\mathrm{i}=1}^{\mathrm{n}} C_{p_i}^{\mathrm{mean}} \left(T_i - T_o - T_o \ln\left(\frac{T_i}{T_o}\right)\right), \quad (2.9)$$

$$C_{p_i^{\mathrm{mean}} = \int_{T_1}^{T_2} C_{p_i} dT,} \quad (2.10)$$

$$C_{p_i}\left(\frac{j}{mol.K}\right) = \mathrm{a_i} + \mathrm{b_i}T + \mathrm{c_i}T^2 + \mathrm{d_i}T^3, \quad (2.11)$$

where a_i, b_i, c_i, and d_i are heat capacity coefficients and *R* is the ideal gas constant [16]. P_i and T_i represent the partial pressure and temperature of individual components respectively at each point in the reactor [19].

Chemical exergy is the largest obtainable work from a matter by taking it from a condition of thermo-mechanical equilibrium to a state of thermo-mechanical and chemical equilibrium with the dead state of the environment [19]. Chemical exergy of a material stream on a molar basis is given by equation 2.12;

$$E^{\mathrm{ch}} = \sum_{\mathrm{i}=1}^{\mathrm{n}} \nu_{\mathrm{i}} \bar{G}_i(\mathrm{Reactants}) - \sum_{\mathrm{i}=1}^{\mathrm{n}} \nu_{\mathrm{i}} \bar{G}_i(\mathrm{Products}), \quad (2.12)$$

$$\bar{G}_i = G_f^0 + [\bar{G}_{i(T,P)} - \bar{G}_{i(To,Po)}], \quad (2.13)$$

where v_i is the respective stoichiometric coefficients, $\bar{G}_i$ is the molar gibbs function of components *i*, and G_f^0 is the molar gibbs function of formation at a reference temperature and pressure [20].

Mixing exergy accounts for the mixing effect arising due to the isothermal and isobaric mixing of pure components at process conditions [21]. It can be calculated by

$$E_{mix} = \sum_{i=1}^{n} x_i T_o R \ln x_i, \quad (2.14)$$

where x_i is a mass fraction of component *i*. Mixing exergy is always a negative value because the mixing of different components decreases the exergy continuously along

the length of the reactor [16]. It can also be written in the form of $\sum_{i=1}^{n} \frac{x_i R T_o \ln p_i}{P_o}$, where P_i is the partial pressure of each component ($P_i = \mathcal{X}_i P_{total}$) according to Dalton's law [22].

Chapter 3

Literature Review and Objectives

This chapter include the literature review regarding the computational fluid dynamic (CFD) technique to quantify exergy, a study of the hydrodynamics, microreactors, and objectives.

3.1 Computational Fluid Dynamics Technique to Quantify Exergy

Farmahini–Farahani (2012) performed an exergy analysis to study the thermal stratification process in a storage tank. Thermal stratification is the layering of water in which hot water rises to the top due to low density while high-density cold water stays at the bottom. Geometrical parameters of tank-like inlet and outlet position, inlet angle, aspect ratio, and inlet and outlet diameter can effect on the level of thermal stratification which can predict through exergetic trends. Thermal stratification is very important industrial phenomena and exergetic analysis can contribute to the optimum design of storage tank [23]. Alabi and Ladeinde (2007) performed an exergy analysis through CFD to optimize the design of aircraft. Exergy analysis identifies the areas of exergy destruction and provides room for the designer to improve the design of aircraft. The results show that exergy destruction and entropy generation is higher on the top part of the aircraft due to the maximum velocity gradient compared to the lower portion of aircraft. The CFD based results are compared with the lumped parametric model. CFD gives a more accurate prediction of exergy analysis than lumped parametric model but it takes more time [24]. Jafarmadar (2015) performed exergy analysis to control the combustion timing of the fuel blends in which fuels have different ignition properties. It is observed that the exergetic efficiency of compressed natural gas is higher than gasoline fuel which shows that CNG has higher work potential. It is also found that exergetic efficiency decreases when the fuel-air ratio increases. This is due to the fact that excessive combustion increases the percentage of carbon dioxide which has low heating value. Hence the overall heating value of products decreases which lower the fuel work potential [25].

3.2 Hydrodynamics Study Through Computational Fluid Dynamics Approach

To determine the flow distributions and pressure drop in packed bed (filters) CFD approach can be very useful. A packed bed filter has a non-uniform distribution of voids. Taylor, et al. (1999) developed a computational model in CFD to analyze the effects of pressure on the void distribution by incorporating the Mueller equation. To deal with turbulence in the bed, standard K-epsilon (two equations) turbulence model was used. A pressure loss is observed in the bed which is determined with the help of the Ergun equation. Through this model, an efficient bed filter can design in which optimum flow distribution is achieved [26].

Membrane reactor is the latest technology to remove nitrogen, organic materials and other wastewater contaminants from water. CFD is a promising approach to enhance the achievments of the membrane reactor. The efficiency of the membrane reactor relies on the mass transfer phenomena which depend upon flow patterns and flow velocity. A tubular hollow membrane is used and a stimulus-response approach is used to investigate the flow patterns. Plascencia-Jatomea, et al. (2015) developed a CFD based model by assuming laminar flow and solve the Navier Stokes equation for incompressible flow. A deviation from ideal hydrodynamic behavior is observed due to mixed flow and channeling effects. With the velocity flow patterns, the stagnant zone is determined in the membrane in which degradation reactions can take place [27]. This stagnant zone can provide the room for improvement of membrane reactor design.

Boulenouar et al. performed CFD-based exergy analysis of flow in a supersonic steam ejector and analyzed that the major irreversibility is created in the nozzle. This is because of the high gradient of velocity and pressure respectively [28]. Mustafa et al. developed a CFD-based model for exergy analysis of naphtha reforming reactors and concluded that the total exergy of the stream increases along the reactor [19]. Alabi et al. studied the experimental and CFD-based exergy analysis methods for the design optimization of the airframe subsystem of aircraft. They observed that exergy-based approach has a large advantage as compared to energy-based approach [29]. Debnath et al. performed CFD-based exergy efficiency analysis of air hydrogen detonation in a pulse detonation combustor. They concluded that the deflagration

combustion process has larger exergy losses than the detonation combustion process [31]. Erguvan et al. analyzed energy and exergy of unsteady cross-flow overheated circular cylinders in the CFD environment. It was found that exergy efficiency can be increased by selecting specific pitch ratios for different Reynolds numbers [32].

3.3 CFD Analysis in Microreactor

Granlund et al. revealed that the micro reactor having multiple air inlets produces a high yield of hydrogen as compared to the conventional monolith reactor by using computational fluid dynamics (CFD) [33]. Bhat et al. presented a review on various research directions in the area of process intensification of the SMR process [34]. Chen et al. developed the CFD-based model of a catalytic micro combustor and evaluated the combustion characteristics and stability of a methane-air mixture [35]. Yu et al. developed the micro reactor for steam reforming of methanol and analyzed the outcomes of the micro reactor with optimum catalyst coating at different operating conditions [36]. Gahui et al. produced a hybrid system of SMR which transforms some part of methane to hydrogen by using the heat of exhaust gases of an internal combustion engine, and they showed through CFD simulation that the homogeneity of temperature in the longitudinal and radial directions is indispensable for high methane conversion efficiency [37]. Yasuki et.al compared the energy requirement for self-heat recuperative systems and conventional thermal processes. They concluded that the recuperative thermal processes have a high capability to save energy than the conventional thermal processes in the industries [38]. Seyed et.al investigated the conventional and flameless combustion in a lab scale furnace on the basis of exergy analysis and Figured out that the major irreversibilities were caused by the high temperature gradient present in the reactor chamber. [39]. An et al. investigated different structures of the micro reactor such as parallel, oblique pin, pinhole, wavy, and coil with CFD simulation to achieve a high-performance configuration with respect to heat transfer, reaction rates, and their flow characteristics. They concluded that the pinhole configuration can achieve better performance than the other structures [40]. Kashid et al. developed a CFD model of slug flow micro reactor to examine the impact of viscosity on the fluid flow streamlines within the slugs. They summarized that the variation in viscosity has no effect on the flow patterns within the slugs [41].

3.4 Exergy Analysis Through Different Tools and their Comparison with CFD

Process design intensively involves process simulators such as Aspen HYSYS/PLUS, CHEMCAD, etc. However, the simulators lack in built-in robust methods for exergy analysis that can be applied to any process being designed. In order to vanish this defect, exergy analysis tools are reproduced in other environments such as FORTRAN, Microsoft Excel, etc., and interfaced with the simulators for analyzing exergy efficiency of the designed process. Querol et al. (2011) integrates Microsoft Excel with Aspen PLUS to calculate exergy and performed exergoeconomis studies of chemical processes [42]. Montelongo-Luna et al. (2011) developed a relative exergy array (REA) to calculate the exergetic efficiency of distillation column [43]. Munir et al. (2013) developed a relative exergy-destroyed array (REDA) to evaluate the economic efficiency of the monochlorobenzene (MCB) plant and a heat exchanger network (HEN) [44]. Hinderink et al. (1996) studied exergy analysis by developing a tool in which an external subroutine (Exercom) is integrated with flowsheeting simulator Aspen PLUS to incorporate the standard chemical exergies of components [21]. Bahmanpour et al. (2014) studied the conversion of methane gas to methanol and methanol to formaldehyde, exergy analysis is performed using Aspen HYSYS and Aspen PLUS [45].

Computational fluid dynamics (CFD) technique is the latest emerging approach to do an exergy analysis of a given system [23, 46]. CFD provides an internal visualization aid compared to other techniques, i.e. Aspen HYSYS/PLUS, CHEMCAD, etc., in which only inlet and outlet exergies are calculated. Huang et al. (2017) investigated the exergy analysis of crystalline nickel ferrite dissociation in a solar reactor and Figured out that physical exergy decreases with the temperature drop. It was noted that a high conversion rate of reaction increases the oxygen production which results in increase of chemical exergy of the process [48]. The space for CFD based exergy analysis of steam methane reforming is still vacant in research work. According to the best of our knowledge, no CFD based exergy analysis of steam methane reforming is performed yet.

3.5 Objectives

In this work, exergy analysis of a monolith micro reactor of SMR was performed by using a computational fluid dynamics (CFD) model. Initially, the CFD model was developed using literature data. The monolith catalyst bed was used by considering its large surface area, low-pressure drop, high durability, and high mechanical strength. The surface based approach was used for modeling reaction rates. In order to incorporate reaction kinetics, the CHEMKIN mechanism was used. Size of the reactor and operation conditions were optimized to realize higher conversion efficiency and smaller capital and operational cost. In order to analyze true thermodynamic efficiency, its exergy analysis of the optimized micro reactor was performed using the custom field function (CFF) integrated with the CFD environment. The optimized catalytic monolith micro reactor of SMR achieved higher conversion efficiency at a smaller consumption of energy, catalyst, and material of construction than the reactor reported in the literature. The exergy analysis algorithm helped in evaluating length-wise profiles of all three types of exergy, i.e., physical exergy, chemical exergy, and mixing exergy, in the micro reactor.

Chapter 4

Procedure of CFD Based Model Development

Computational fluid dynamics (CFD) is the science of discussing fluid flow, heat transfer, mass transfer, chemical reactions, and the phenomena related to all, by solving the mathematical equations which describe these processes by using a numerical process. To perform the calculations, computers are required to simulate the gases and liquids interaction with surfaces described by boundary conditions. Quick solutions can be achieved through high-speed supercomputers. Various softwares are developed through continuous research which are highly efficient and accurate in solving the complex simulation problems such as turbulent and transonic flows. The results of CFD analyses are used in conceptual studies of new designs, detailed product development, trouble shooting, and redesign of processes.

4.1 Background

Navier-Stokes equations are the fundamental of all CFD problems and these equations define many single-phase fluid flow problems. To simplify these equations, viscous terms are removed to yield the Euler equations. To simply further these equations and yield potential equations, vorticity terms are removed. Finally, linear potential equations are obtained by removing the subsonic and supersonic flow terms.

Earlier Lewis Fry Richardson divided the physical space into cells and apply finite different method which resembles with modern CFD calculations. Although he failed to get the required results, later these calculations which he mentioned in his book “Weather prediction for numerical process” provide the basis for modern CFD calculations.

4.2 Methodology

4.2.1 Preprocessing

The preprocessing consists of the following steps:

- Computer-aided design (CAD) can be used to define the physical boundary and geometry of the problem. From there, the fluid volume is calculated.
- The volume which is covered by the fluid is then divided into small cells (mesh). The mesh may be the same overall or non-uniform, pyramidal or polyhedral, tetrahedral, structure or unstructured cells.
- Now the physical mesh is defined using fluid motion, radiation, enthalpy, and species conservation or non-conservation equations.
- Boundary conditions are specified.

4.2.2 Processing

Simulations are processed until the convergence is reached and the different equations are solved as a steady state condition or a transient state.

4.2.3 Post Processing

Finally, the post-processing is done to observe the results visually and can analyze the solution.

4.3 Simulation Environment

4.3.1 Design Modeler 16.0

There are many geometries making software such as Design modeler, Gambit, Solid Works, Auto CAD, IGES, etc. Design modeler is very basic and user-friendly software compares to others. Design modeler was used for making the geometry. In this work, two-dimensional geometry was prepared with the help of vertices. Vertices were connected with each other to form the edges which were further used to form the faces. Structured meshes were prepared and boundary conditions were labeled at the edges while different zones were labeled at the faces. GUI of design modeler is shown in Figure 4.1.

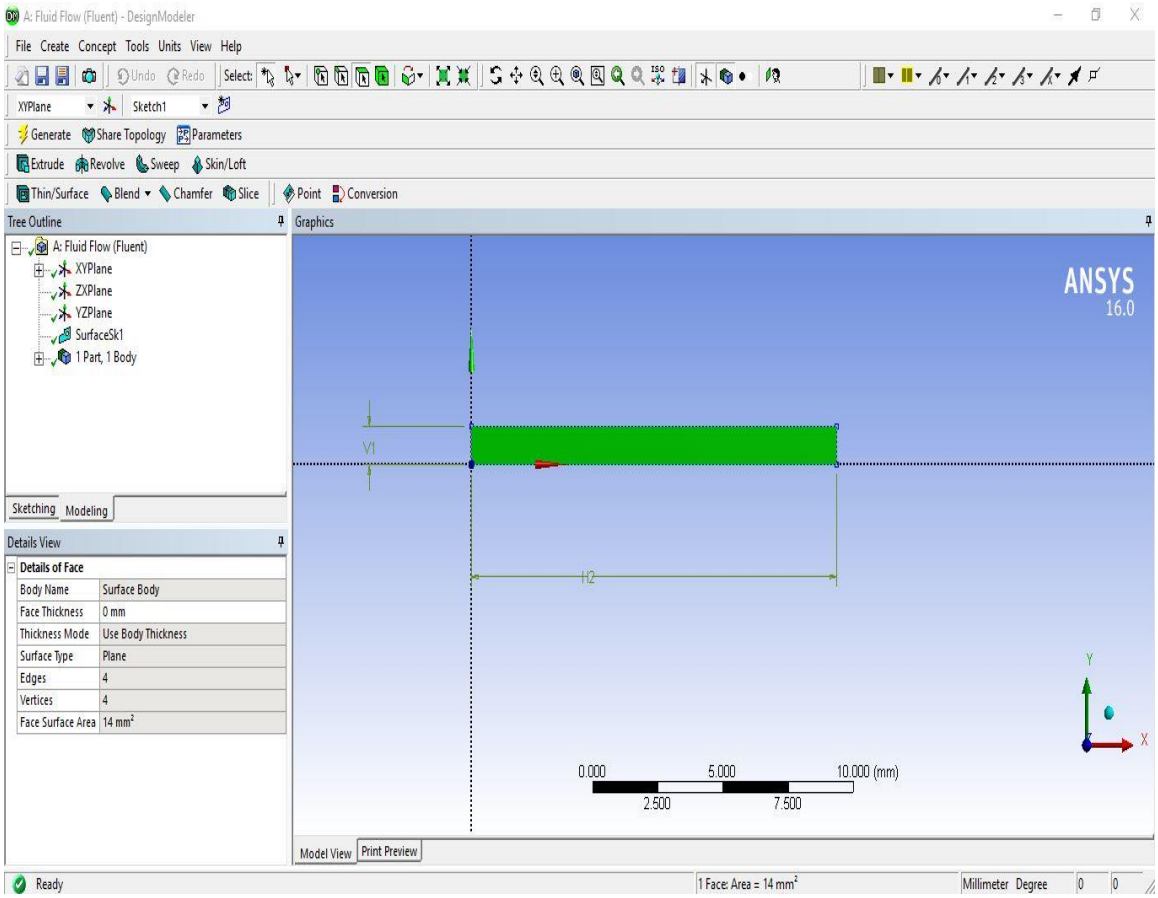

Figure 4.1: Geometry of monolith reactor by design modeler

4.3.2 ANSYS Fluent

Geometry was exported from design modeler to the fluent software which performs required simulation. Control volume method was used to solve the mass, energy, and species conservative equations. Mesh quality was calculated in ANSYS Fluent. The boundary and zone conditions which were labeled in design modeler CFD software, were specified one by one in Fluent. Under the solution method, pressure velocity coupling scheme was chosen and specified the discretization for gradient, pressure, momentum, turbulent kinetic energy and species. Under the solution control method, relaxation factors were adjusted for pressure, velocity, density, and other parameters. Residual monitors for absolute convergence were specified to find out the absolute convergence. After that initialization of solution was carried on and then iteration was performed at different equations until the absolute convergence was achieved. Figure 4.2 shows the GUI of the Fluent tool.

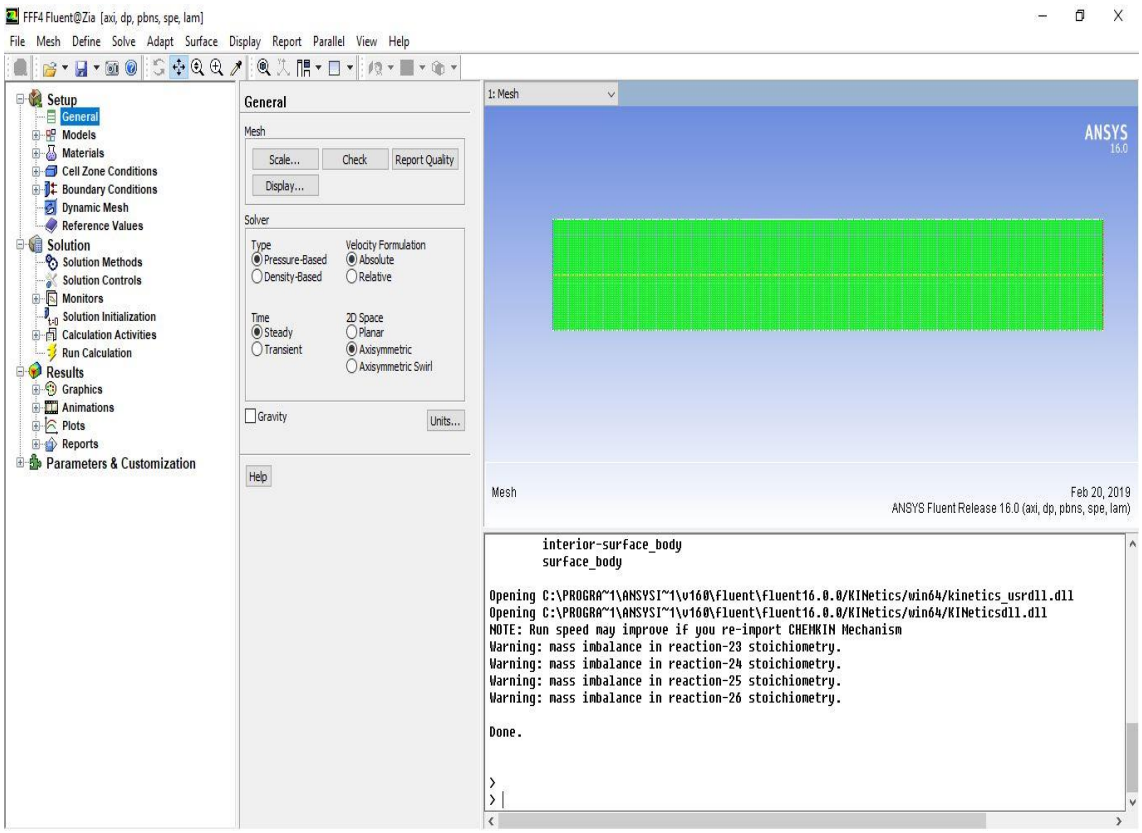

Figure 4.2: Ansys Fluent environment

Four reaction models; laminar finite-rate, finite-rate/eddy-dissipation rate, eddy-dissipation, and eddy-dissipation concept are present in the fluent to deal with reactions and incorporate turbulence-chemistry interactions. In laminar finite-rate, Arrhenius expressions are used to calculate reaction rate and turbulence effects are ignored. In the finite-rate/eddy-dissipation rate, both Arrhenius expression and mixing can influence the reaction. In eddy-dissipation model, the reaction rate is controlled and determined by turbulence while in the eddy dissipation concept model, Arrhenius expression is also incorporated in turbulent flames. Laminar finite-rate model is used due to the low flow velocity i.e. 0.45 m/sec in Arrhenius chemical kinetics. The values of different reaction parameters in these reaction models which includes pre-exponential factor, activation energy, mixing law constants, stoichiometric coefficients and rate exponent are required to incorporate different reactions as shown in Figures 4.3 and 4.4 respectively.

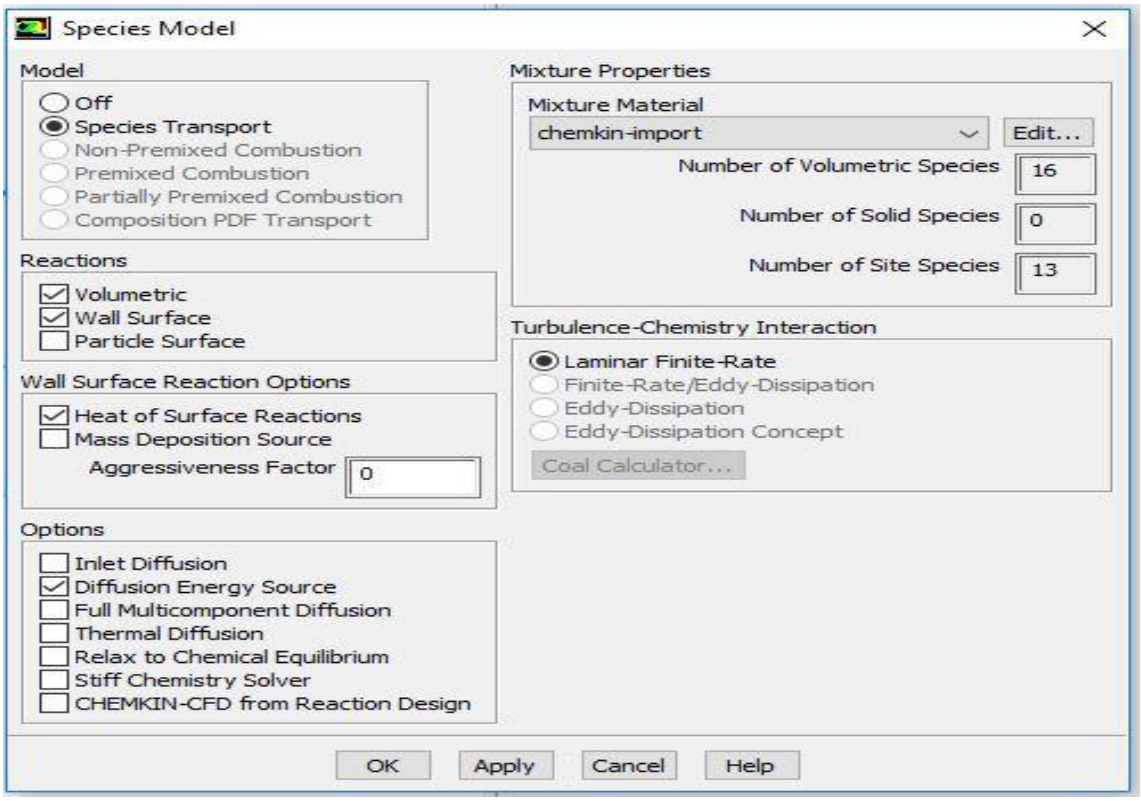

Figure 4.3: Reaction Model

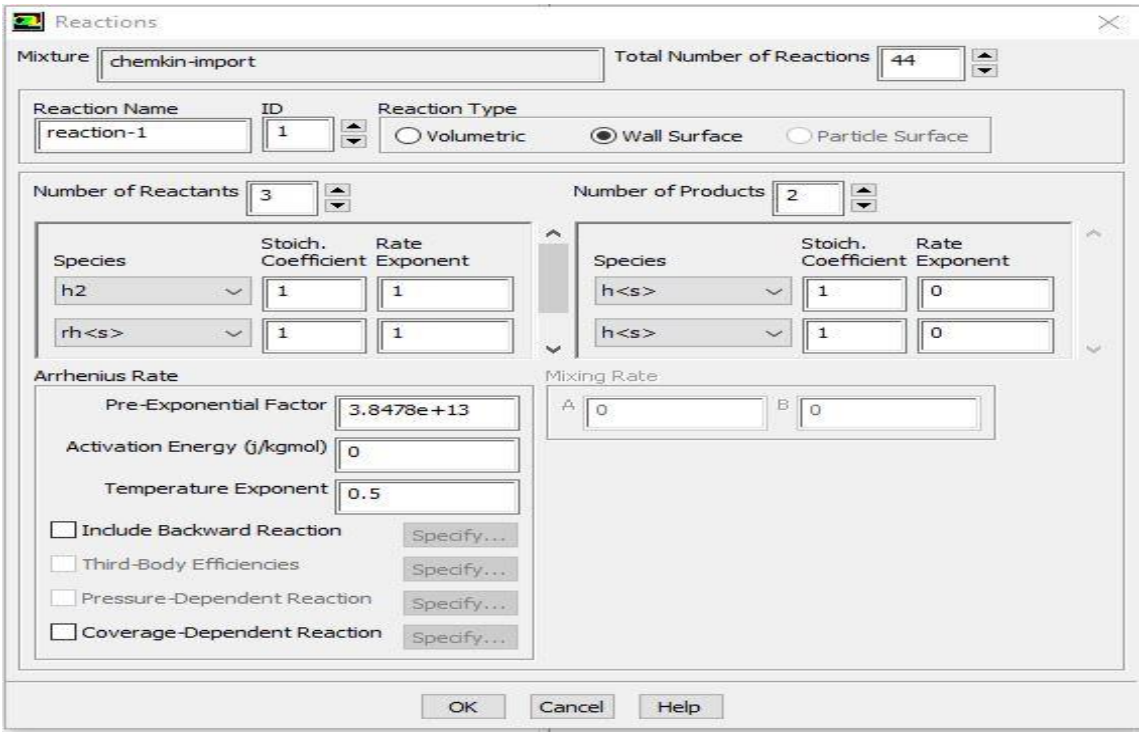

Figure 4.4: Reaction Parameters

4.3.3 Reading of Formulas Through Custom Field Function.

Computational fluid dynamics are basically developed for aerodynamics and mechanical engineers to analyze the stress and strain analysis of different equipment under different conditions. To solve the problem of chemical engineering in CFD, some components, formulas, and reactions are not present in the database of Ansys Fluent which required the external interface through coding. In this work, we use the custom field function to import the exergy formulas and use the chemkin file to read the different reaction into fluent and this is shown in the Figures 4.5 and 4.6 respectively.

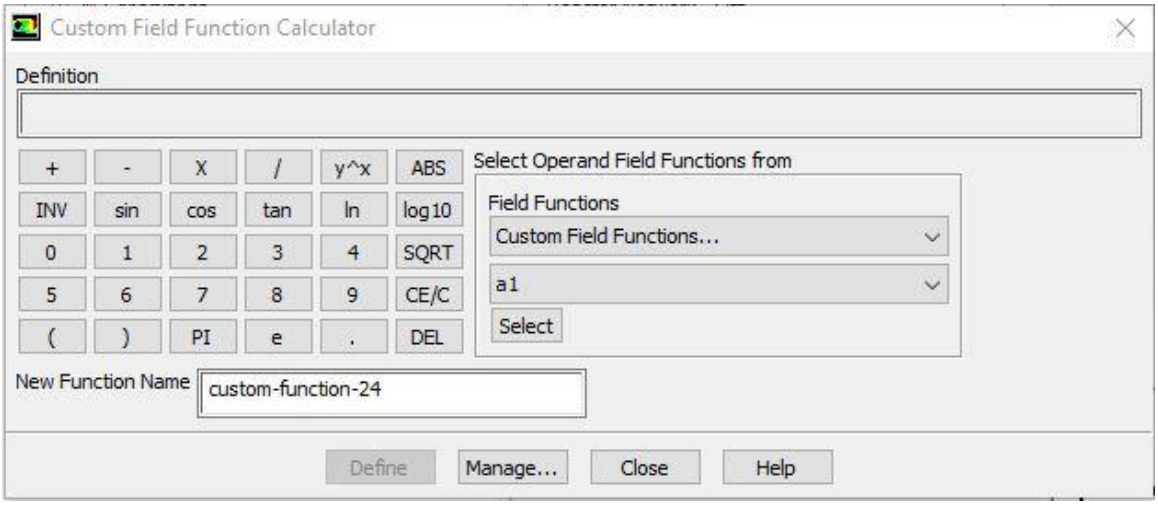

Figure 4.5 Custom field function calculator

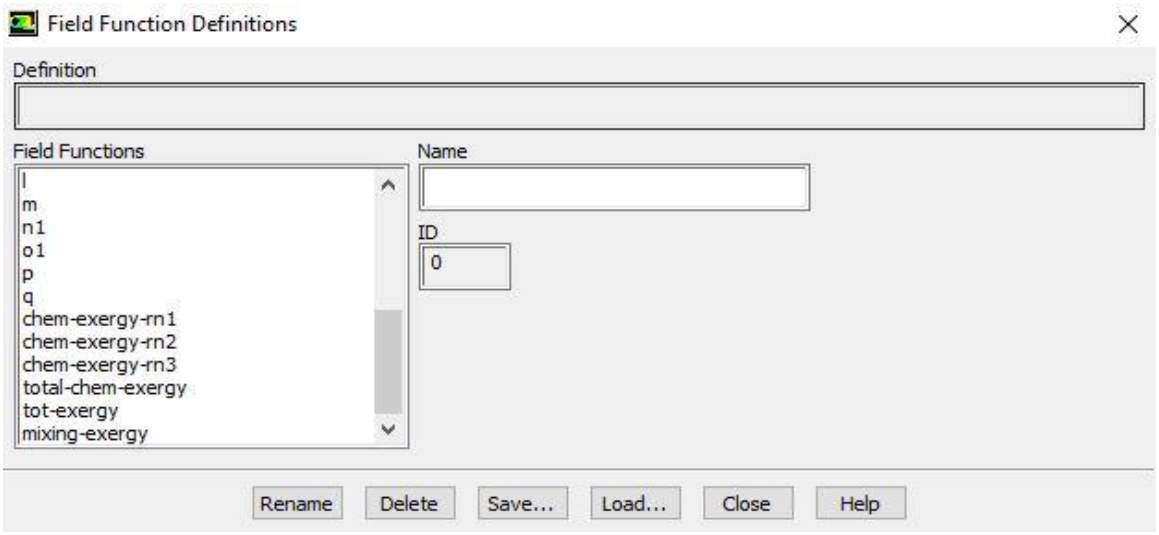

Figure 4.6 Field function definitions

4.3.4 Convergence Criteria

The commonly used convergence criteria for the residuals of continuity, x-velocity, y-velocity, epsilon, and species equation are .001 while criteria for convergence of energy equations are 1e-06. To achieve convergence, the absolute convergence criteria need to be satisfied. To adjust the values of convergence the Figure 4.7 shown the setting monitors.

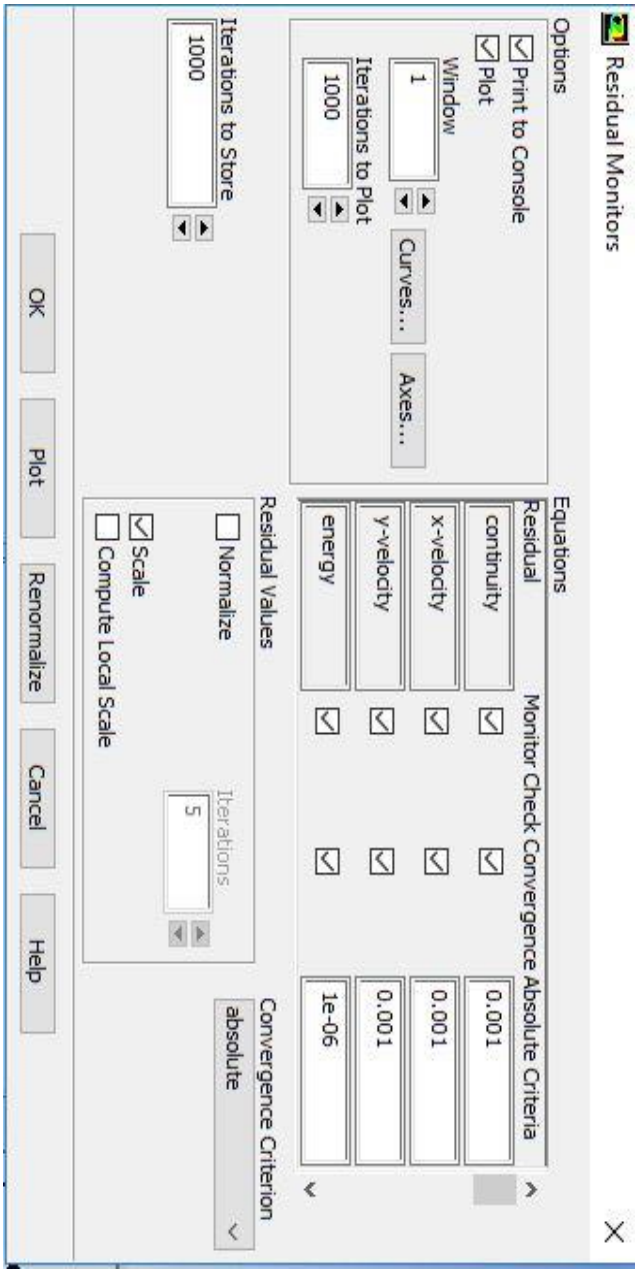

Figure 4.7: Residual monitors sittings

The solution of my problem is converged with 2196 iteration as shown in Figure 4.8 and 4.9 respectively.

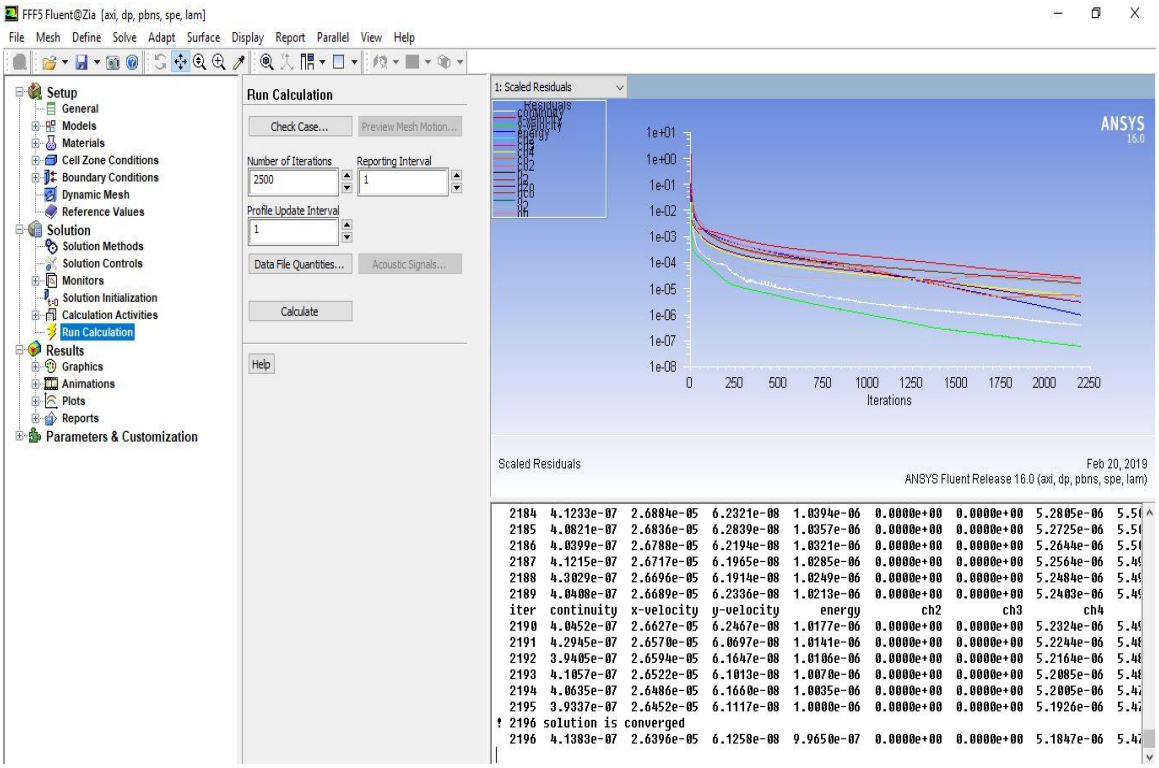

Figure 4.8: Residual monitor

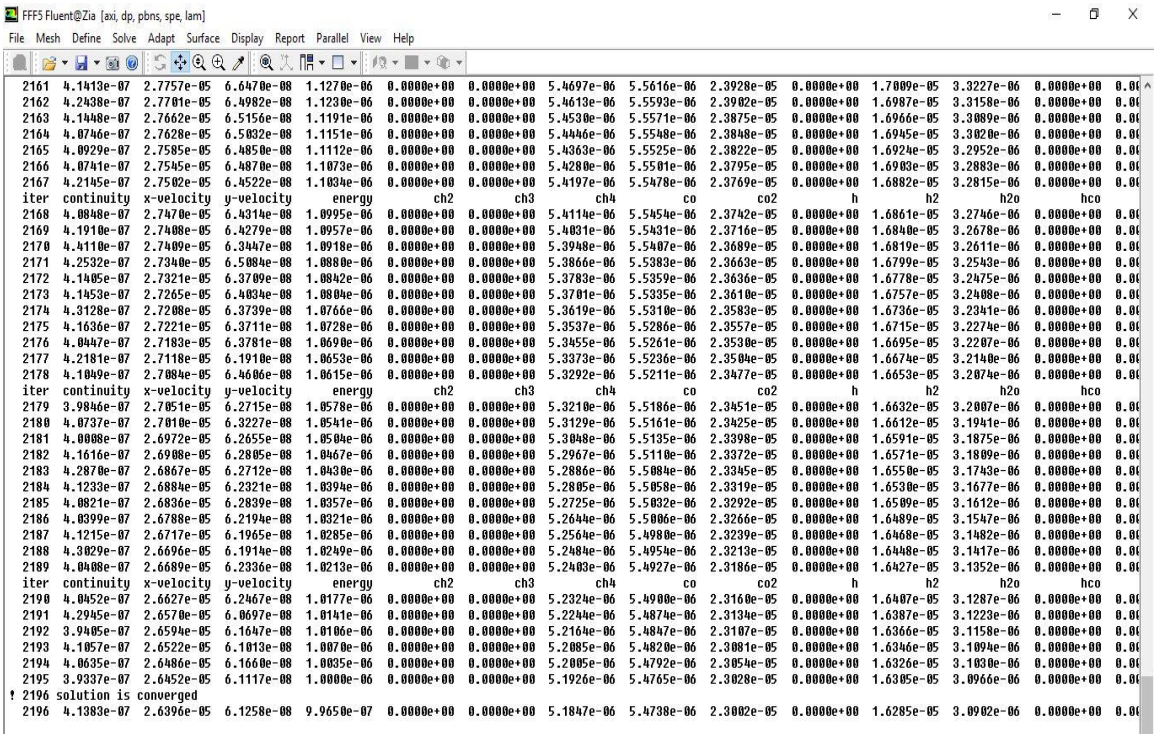

Figure 4.9: Iteration monitor

Chapter 5

Model Development

In section 5.1, details regarding geometry and mesh preparation are provided while in section 5.2, identification of boundary and cell zone conditions is mentioned. A set of CFD based conservative equations is referred in section 5.3 and to solve these equations different numerical schemes are used which are given in section 5.4. Following are the assumptions for model development:

- The equilibrium state is reached and the maximum yield is achieved.
- There is a negligible loss of heat from the wall of reactors to the environment.
- The catalytic wall is isothermal in condition.
- The flow is laminar in the reactor and steady-state condition is achieved.
- The gas mixture is incompressible and considers an ideal gas. The mixture density is considered constant and calculated from ideal gas law.

5.1 Geometry and Meshing

The ANSYS Design Modeller was used to create geometry and mesh. The reactor considered in this study is cylindrical in shape, with a height of 1 mm and length of 14 mm. The reactor consists of an isothermal catalytic (Rhodium catalyst) wall as shown in Figure 5.1. Axisymmetric mesh is used for the simulation; for effective visualization, the axisymmetric mesh was mirrored around its axis. The zoomed version of the mesh is shown in Figure 5.2. The computational mesh consists of 7200 cells and 7525 nodes. Three important parameters to evaluate the mesh quality are minimum orthogonal quality, maximum ortho-skew, and maximum aspect ratio; they are 1.0, 0.0, and 1.4, respectively. Table 5.1 presents the mesh properties.

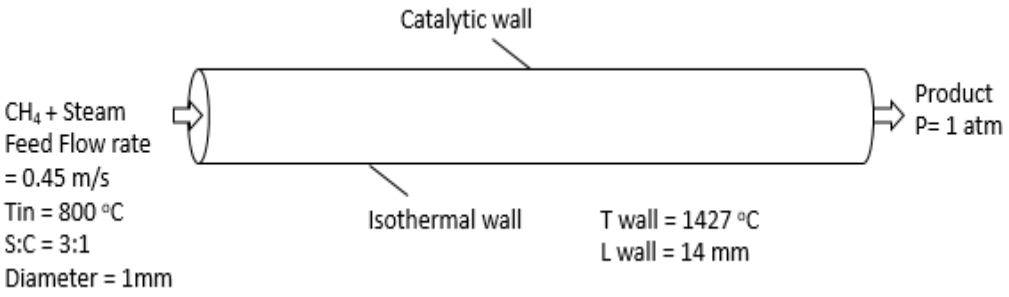

Figure 5.1: A single tube of a monolith catalyst reformer

Table 5.1: Values of different mesh properties

Properties of mesh	Values
Orthogonal quality (minimum)	1.0
Ortho skew (maximum)	0.0
Aspect ratio (maximum)	1.4
The number of nodes	7525
The number of cells	7200
Minimum volume (m3)	2.4e-13
Maximum volume (m3)	2.3e-11
Total volume (m3)	4.2e-08
Minimum face area (m2)	4.1e-05
Maximum face area (m2)	4.5e-05

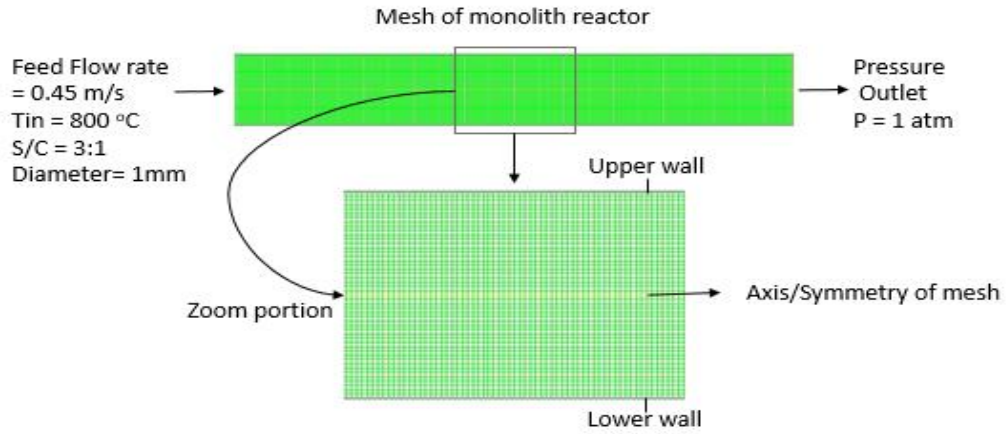

Figure 5.2: Computational grid of monolith reactor and zoom portion of the grid

5.2 Boundary and Cell Zone Conditions

A single tube of monolith reactor is shown in Figure 5.1 Boundary conditions were defined at the inlet and outlet of the reactor. The inlet boundary condition, i.e., the velocity, temperature, pressure, and the composition of inlet gas mixture, in each channel is set at uniform values. The catalytic wall of the reactor tube is kept isothermal. Rhodium (Rh) catalyst is pasted at the inner side of every single reformer tube. It facilitates the generation of hydrogen fuel from steam and methane through the SMR reactions. It also assists as an intermediate medium to make the heat transfer rates higher to the tube-side gas mixture in the simulations [7]. The flow is considered as a continuous medium and therefore there is no slip conditions on the micro reactor walls. The mixture at the outlet is expelled to an atmospheric pressure. Table 5.2 shows the model boundary conditions.

5.3 CFD Conservative Equations

Finite volume method with cell centered configuration is used to discretize the species, energy, continuity and momentum equations. Computational control volumes are used to demonstrate the conservation laws. Conservation laws are executed on each control volume and across the domain using species transport, energy conservative, continuity, and momentum equation.

Table 5.2 Model boundary conditions

Parameters	Symbol	Value
Channel Length	L	14mm
Channel Diameter	D	1mm
Inlet Temperature	T_{in}	800°c
Isothermal wall temperature	T_w	1427°c
Pressure	P	1 atm
Ratio of Steam to Carbon	S/C	3:1
Inlet Velocity	V_{in}	0.45m/s
Number of Catalyst active site	Γ	$2.7e^{-9}mol/cm^2$

5.3.1 Species Transport Equation

$$\frac{\partial(\rho Y_i)}{\partial t} + \frac{\partial(\rho u_x Y_i)}{\partial x} + \frac{\partial(\rho u_y Y_i)}{\partial y} = -\left[\frac{\partial J_{i,x}}{\partial x} + \frac{\partial J_{i,y}}{\partial y}\right] + \dot{S}_i, \tag{5.1}$$

$$J_{i,x} = -\rho D_i \frac{\partial Y_i}{\partial x}, \tag{5.2}$$

$$J_{i,y} = -\rho D_i \frac{\partial Y_i}{\partial y}, \tag{5.3}$$

where Y_i is a mass fraction, D_i is a diffusion coefficient, J_i is a mass flux of component *i*, and $\dot{S}_i$ is the net production rate of species through chemical reactions [49]

5.3.2 Energy Conservative Equation

$$\rho \frac{De}{Dt} = -P\ div\ u + div\ (k\ grad\ T) + \phi + Si, \tag{5.4}$$

$$div\ u = \frac{\partial u_x}{\partial x} + \frac{\partial u_y}{\partial y}, \tag{5.5}$$

$$grad\ T = \frac{\partial T}{\partial x} + \frac{\partial T}{\partial y}\,, \tag{5.6}$$

$$e = C_v T\,, \tag{5.7}$$

$$P = \rho R T, \tag{5.8}$$

$$\phi = \mu\left\{2\left[\left(\frac{\partial u_x}{\partial x}\right)^2 + \left(\frac{\partial u_y}{\partial y}\right)^2\right] + \left(\frac{\partial u}{\partial y} + \frac{\partial v}{\partial x}\right)^2\right\}, \tag{5.9}$$

where e is the internal energy per unit mass, C_v is specific heat constant, k is the thermal conductivity. ϕ shows the rate of dissipation energy per unit volume and s denotes the work done per unit volume by body forces. The first term of the RHS of the Equation 5.4 is the rate of work done per unit volume, and the second term is the rate of heat transfer per unit volume through conduction [50].

5.3.3 Continuity Equation

$$\frac{\partial \rho}{\partial t} + \frac{\partial (\rho u_x)}{\partial x} + \frac{\partial (\rho u_y)}{\partial y} = \mathrm{S_m}\,, \tag{5.10}$$

where ρ, u_x, and u_y are the density, velocity in x, and y-direction respectively. S_m represents a mass addition to the continuous phase which is zero in this case. The first term of the LHS of the equation shows local derivative which is the change of density per unit time at the fixed point. The second and third terms show the convective derivative of the density of the gas mixture [51].

5.3.4 Momentum Equation:

$$\frac{\partial (\rho u_x)}{\partial t} + \frac{\partial (\rho u_x u_x)}{\partial x} + \frac{\partial (\rho u_x u_y)}{\partial y} = -\frac{\partial P}{\partial x} + \frac{\partial}{\partial x}\left[\frac{4}{3}\mu\frac{\partial u_x}{\partial x} - \frac{2}{3}\mu\frac{\partial u_y}{\partial y}\right] + \frac{\partial}{\partial y}\left[\mu\left(\frac{\partial u_y}{\partial x} + \frac{\partial u_x}{\partial y}\right)\right], \tag{5.11}$$

$$\frac{\partial(\rho u_y)}{\partial t}+\frac{\partial(\rho u_y u_x)}{\partial x}+\frac{\partial(\rho u_y u_y)}{\partial y}=-\frac{\partial P}{\partial y}+\frac{\partial}{\partial y}\left[\frac{4}{3}\mu\frac{\partial y}{\partial y}-\frac{2}{3}\mu\frac{\partial u_x}{\partial x}\right]$$

$$+\frac{\partial}{\partial x}\left[\mu\left(\frac{\partial u_y}{\partial x}+\frac{\partial u_x}{\partial y}\right)\right], \qquad (5.12)$$

where *P* represents the stream pressure and μ is the viscosity of the gas stream. The first term of the RHS of each equation shows pressure forces. The second and third terms of the RHS of each equation show the viscous forces [49].

5.4 Computational Schemes

The governing equations, i.e., momentum, energy, continuity, and species conservation, were discretized by using the finite volume method and were solved numerically by FLUENT 16.0. The second-order upwind scheme was used to discretize the mathematical model. The semi-implicit method for pressure linked equations (SIMPLE) algorithm was used. Exergy analysis was performed by developing a Custom Field Function (CFF) based algorithm. An under-relaxation factor was used to slow down the rate of change. The default reference frame was used for velocity initialization. The Mach number, the ratio of flow velocity to the speed of sound, was used to determine whether the flow is compressible or incompressible. The Mach number was less than 0.3 in our model due to the low velocity of the gas stream; consequently, compressibility effects were ignored and a pressure-based solver was used. Furthermore, the laminar finite rate model was used for calculating the rate of reactions. Computations are very intensive, and the convergence of CFD simulations was evaluated based on the residuals of all governing equations. The governing equations in our CFD model were converged at 2196 number of iterations as shown in Figure 4.8.

A schematic flowchart of the methodology adopted in this study is shown in Figure 5.3. Model development starts with geometry preceded by mesh preparation and identification of the boundary and zone cell condition. Then, the ANSYS Fluent simulator reads the mesh and its properties. As temperature variations occur due to reaction kinetics, the energy equation was enabled in ANSYS Fluent to analyze the

effect of temperature. Reaction kinetics and reaction thermodynamics were imported through the CHEMKIN file. The formulas for physical, chemical, mixing, and total exergy were generated and imported to the ANSYS Fluent software through the CFF. Changes in a mole fraction of species and exergy profiles were evaluated.

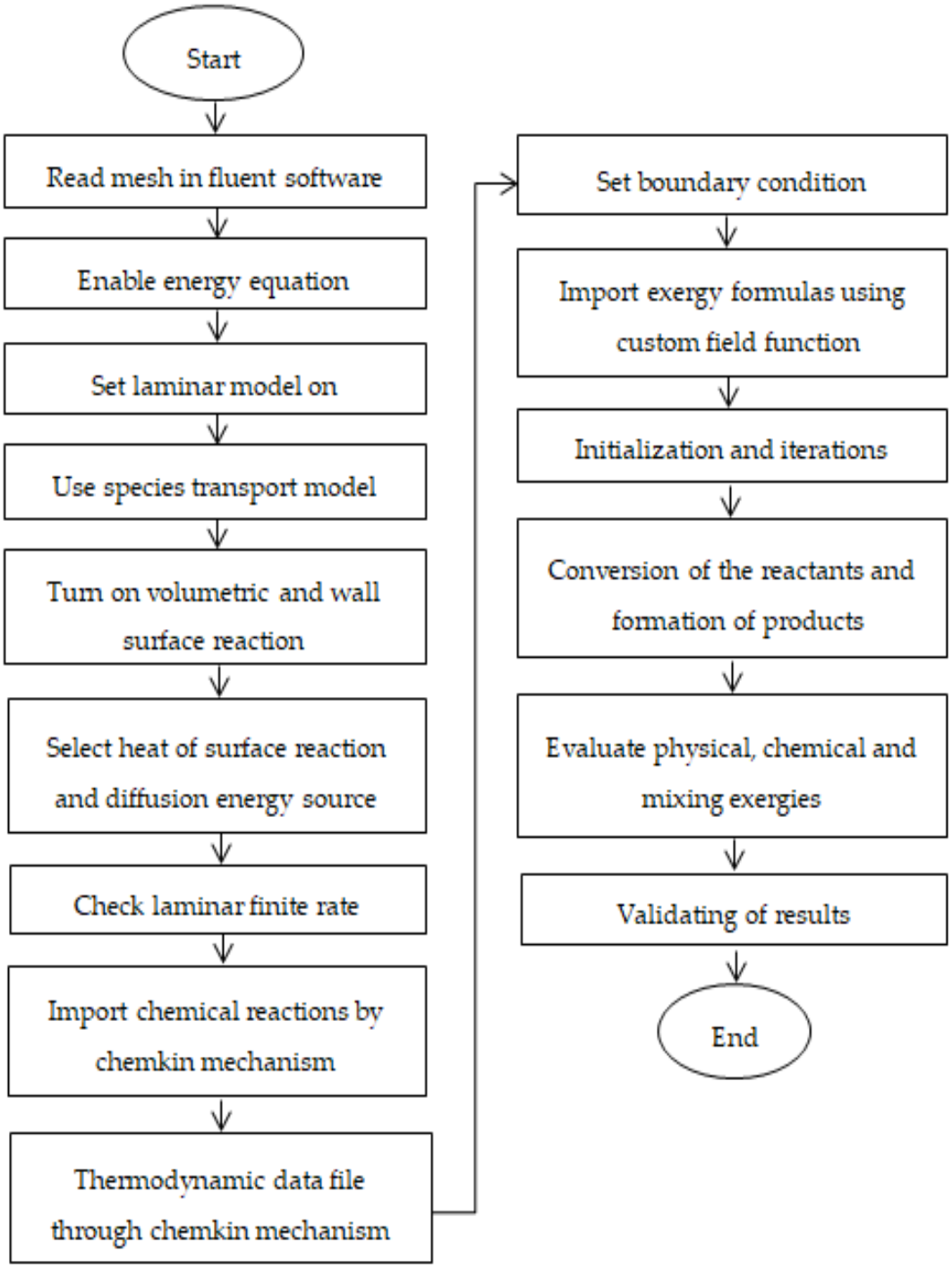

Figure 5.3: Schematic of model development process

Chapter 6

Results and Discussion

The results and discussion encompass contours and profiles of temperature, pressure, mole fractions of reactants and products, and exergy profiles of the reactor model. Contours of temperature, pressure, mole fractions of reactants, and products are shown in Figure 6.1. While the contours of three types of exergy and total exergy are shown in Figure 6.2. The profiles of temperature and pressure are shown in Figures 6.3 and 6.4, respectively. While the mole fractions of methane, steam, hydrogen, and carbon monoxide are shown in Figure 6.5. Mixing exergy profile is demonstrated in Figure 6.6, followed by Physical, chemical, and total exergy profiles in Figure 6.7.

The temperature contours and profile are shown in Figures 6.1 and 6.3, respectively, portrays the change in temperature in the longitudinal direction. A constant amount of heat is supplied through the wall of the reactor where the temperature drops in the first part of the reactor, i.e., up to 8mm, due to the consumption of heat in an endothermic reaction. On the completion of the reactions, in the later part of the reactor, i.e., up to 14 mm, less amount of heat is consumed and the temperature remains high and constant.

Figure 6.1 and 6.4, shows the pressure contours and its graph respectively, reveals the decreasing trend linearly along the length of the reactor. The continues pressure drop is due to the increase of fluid velocity along the length of the reactor. The increase in velocity causes the pressure drops inversely in fluids. The same effect is stated by the Bernoulli equation.

The contours and the graph of methane conversion are shown in Figure 6.1 and 6.5, respectively, portrays that the mole fraction is decreasing rapidly from 0.23 to 0.083, i.e., up to 12mm, then remains constant. Methane is limiting reactant and it is converted up to 63%. In a previous study reported in the literature, 60% conversion of methane was achieved in a monolith reactor. The conversion of excess reactant,

i.e., steam, is shown in Figures 6.1 and 6.5, respectively, where the mole fraction of steam drops from 0.77 to 0.57.

The formation of hydrogen is shown in Figure 6.1 and 6.5, respectively, demonstrate that the concentration of hydrogen increases along the length of the reactor up to 9mm. Then a slight decrease was noticed up to 12mm. The decrease in concentration may be caused by the formation of intermediates and reversible reactions shown in Table 2.2. Similarly, the concentration profile of carbon monoxide is shown in Figures 6.1 and 6.5, respectively, where the concentration of carbon monoxide is continuously increasing along the length of the reactor.

The performance of the proposed model is compared, with a model reported by Cao et al. in the literature [49]; see Table 6.1. The proposed model achieved a 7.4% higher conversion with 76.6 % smaller surface area compared to the reported work [49]. The higher conversion at the shorter reactor is due to a higher wall temperature, i.e., 1477 ^{o}C, in the proposed work compared to 900 ^{o}C, in the reported work. However, total heat consumption in the proposed model is 65.0% lower than the reported work due to the smaller surface area. Furthermore, the reduction in the size of the reactor resulted in a 76.7% lesser requirement of the catalyst in comparison with the reported work [49].

The mixing exergy always has a negative value as exergy of pure components is higher than the components in the mixed form [16]. Decrease in total exergy due to mixing is demonstrated in Figure 6.2 and 6.6, respectively. The high conversion rate in the reactor produces new product species at a faster rate. The high-speed molecules intensify the mixing effects. These effects create major irreversibility and contribute significantly to the overall exergy destruction in the reactor. This trend of mixing exergy is validated by another study reported in the literature [19].

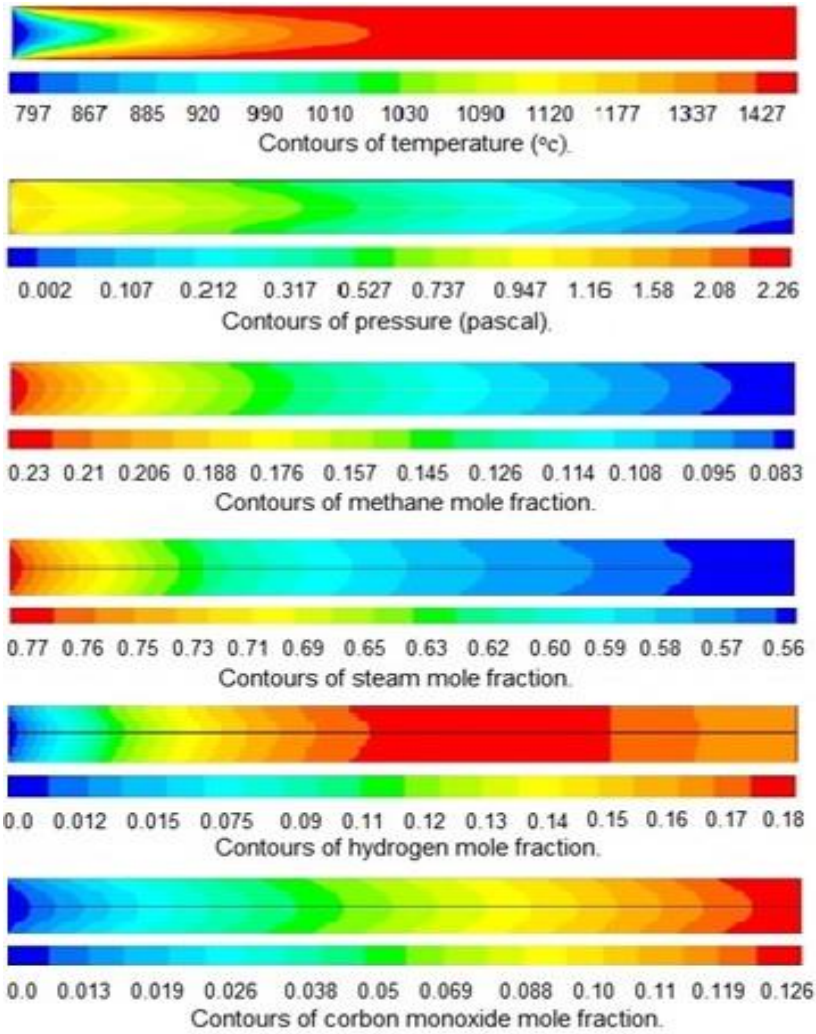

Figure 6.1: Total Contours of simulation results along the length of the reactor (0-14mm).

The contour and profile of physical exergy are shown in Figures 6.2 and 6.7, respectively. At the start of the reactor, the quantity of physical exergy is low which then increases rapidly up to 7 mm. The low quantity of physical exergy at the start of the reactor is due to the low temperature as shown in Figures 6.1 and 6.3, respectively. The low temperature is due to the consumption of heat by endothermic reactions of steam methane reforming. The temperature drop causes irreversibility which results in a decrease in physical exergy at the start of the reactor. The slight decrease in the physical exergy from 7 mm to 12 mm is noticed which is caused by the continued decrease of pressure from start to end of the reactor; physical exergy at this portion only depends on the pressure because its temperature remains constant.

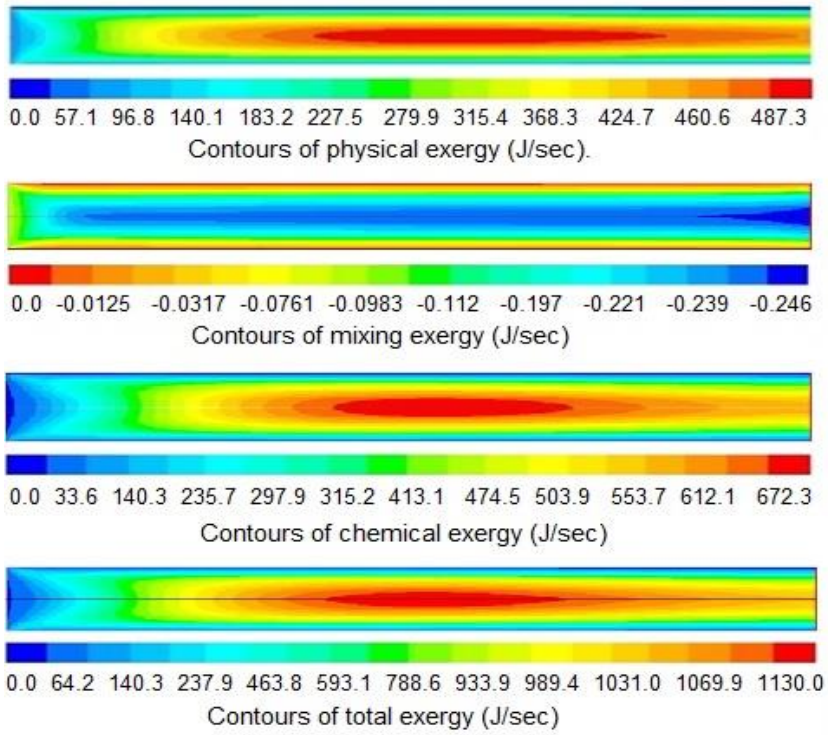

Figure 6.2. Contours of three types of exergies and total exergy, along the length of the reactor (0-14mm)

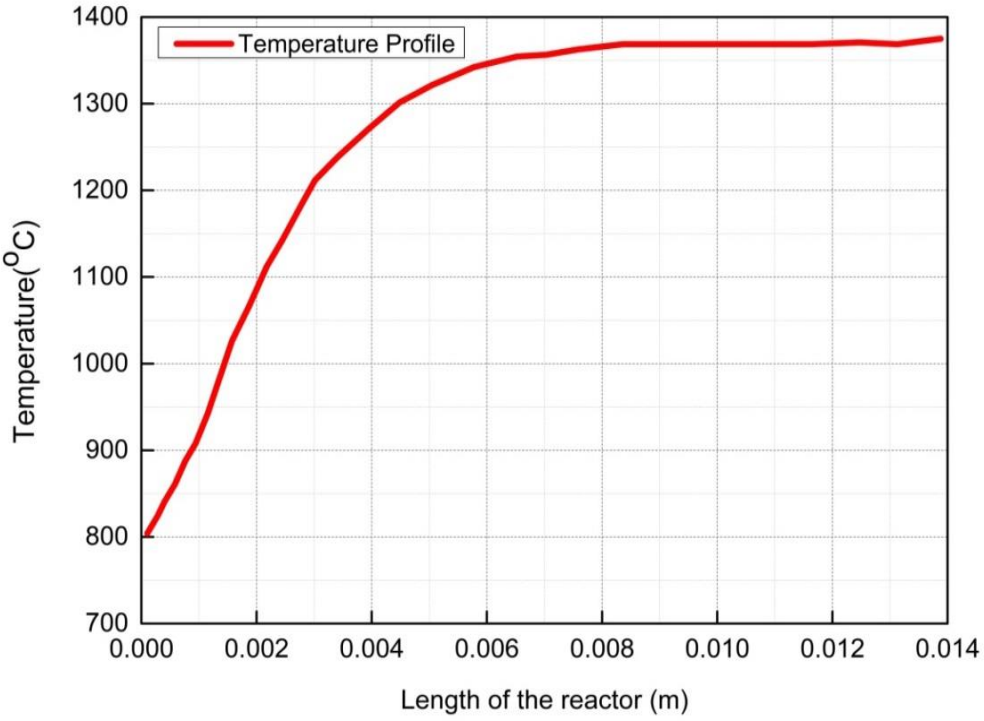

Figure 6.3: Temperature profile along the length of the reactor

The contours and profile of chemical exergy increases from left to right of the reactor as shown in Figures 6.2 and 6.7, respectively. Chemical reactions take place in catalytic bed and produce new species. These species have high chemical potential which increases the total chemical exergy.

Total exergy is the summation of physical, mixing, and chemical exergy which is shown in Figures 6.2 and 6.7, respectively. The total exergy increases from the start of the reactor till the end of the reactor. The increase in total exergy is due to the combine increasing effect of physical and chemical exergies. The increase in total exergy results in higher work potential of the product, syngas.

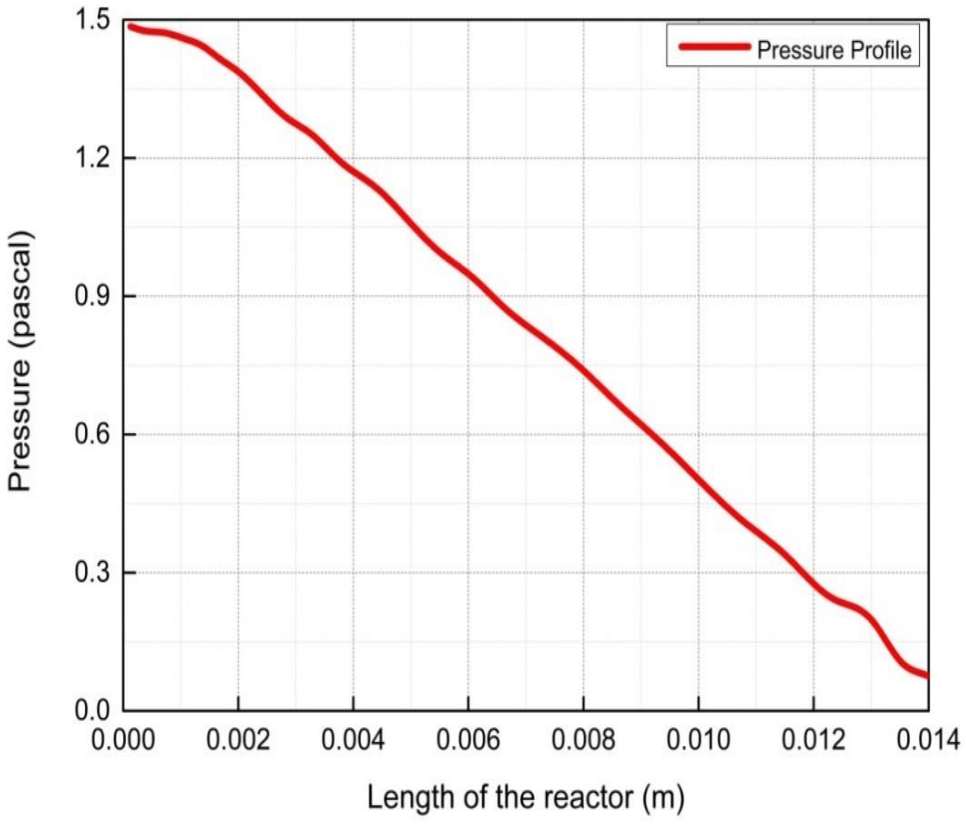

Figure 6.4: Pressure profile along the length of the reactor

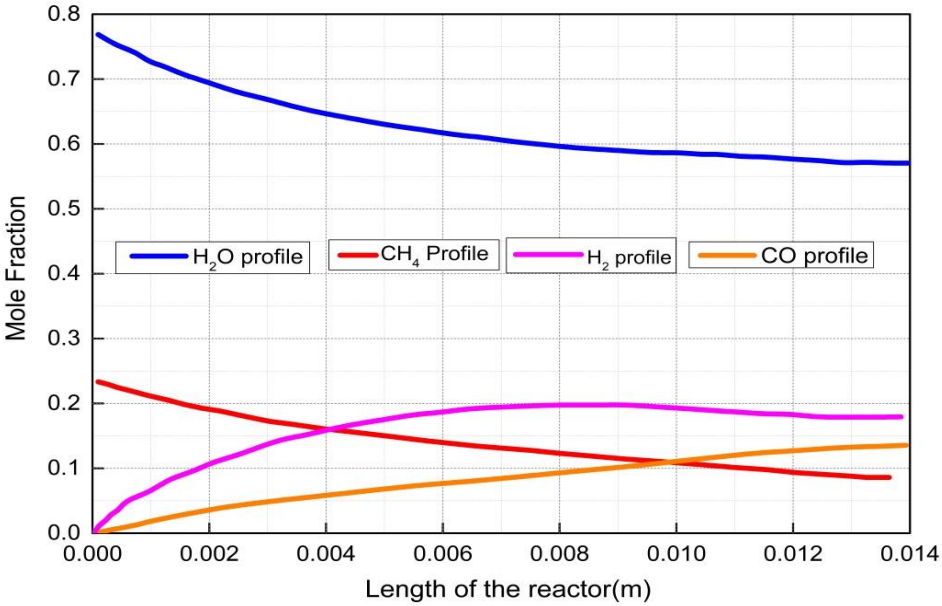

Figure 6.5: Conversion profiles of the reactants and formation of the products along the length of the reactor

Table 6.1 Comparison of the proposed model with the model reported in the literature [49].

Parameters	**Literature data**[49]	**Proposed model data**
Feed temperature	800 ^{o}C	800 ^{o}C
Wall temperature	900 ^{o}C	1477^{o}C
Pressure	1 atm	1 atm
Steam to methane ratio	3:1	3:1
Inlet velocity	0.45 m/s	0.45m/s
Length	6.0×10^{-2}m	1.4×10^{-2}m
Surface area	1.88×10^{-04} m^2	4.4×10^{-05} m^2

Heat requirement	22.05 kW	7.7 kW
Conversion	60 %	67.4 %
Catalyst requirement per length	5.076×10^{-09} moles	1.18×10^{-09} moles

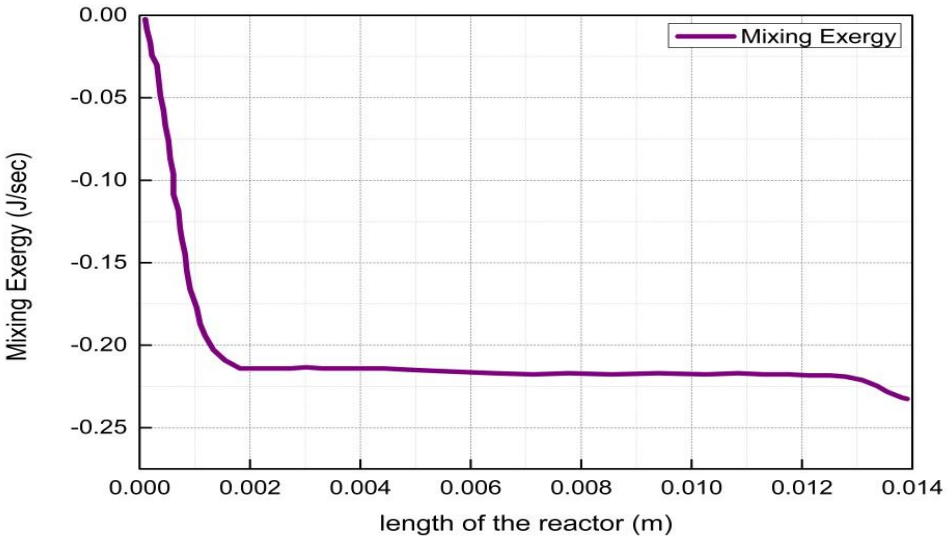

Figure 6.6: Mixing exergy profile along the length of the reactor

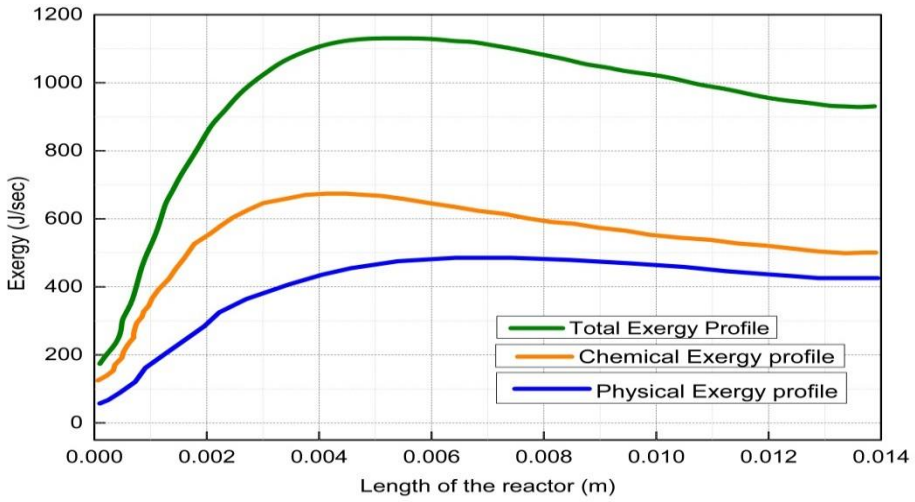

Figure 6.7: Profiles of two types of exergies and total exergy along the length of the reactor

Conclusions and Recommendations

In this work, the computational fluid dynamics (CFD) based method was adopted to perform exergy analysis of the monolith micro reactor of the steam methane reforming (SMR) process. Initially, the CFD model of SMR was developed using literature data. In order to incorporate reaction kinetics, CHEMKIN was used. By optimizing the size and the operation condition, the optimal SMR micro reactor achieved a 7.4% higher conversion with 76.6 % smaller surface area compared to the reported work. The higher conversion achieved by the shorter reactor is due to a higher wall temperature, i.e. 1477 ^{o}C, in the proposed work compared to 900 ^{o}C in the reported work. Although the temperature used in the proposed work is higher than the reported work, total heat consumption in the proposed work is 65.0% lower due to the smaller surface area. Furthermore, the reduction in the size of the reactor resulted in a 76.7% reduction in the catalyst requirement.

The exergy analysis was performed by developing the custom field function (CFF) based algorithm. The exergy analysis helped in evaluating length-wise profiles of all three types of exergy, i.e., physical exergy, chemical exergy, and mixing exergy, in the micro reactor. The results showed that the physical and chemical exergy increases due to the increase in temperature and high chemical potential of product species, respectively. On the other hand, mixing exergy decreases due to the high rate of mixing effects that causes irreversibility.

In future work, sensitivity analysis and uncertainty analysis can be performed to realize further optimization of the process conditions. The sensitivity analysis helps in evaluating the individual impact of process conditions on its outcome, while the uncertainty analysis is used to quantify the collective impact of variation in process conditions on its outcome.

Appendix

Exergy Codes

(define/custom field function)

physical exergy = ((21.725 * (ln (total-pressure / 101325)) * (axial-velocity / total-temperature)) * (molef-ch4))+ (21.725 * (ln (total-pressure / 101325)) * (axial-velocity / total-temperature)) * (molef-h2o))+ (21.725 * (ln (total-pressure / 101325)) * (axial-velocity / total-temperature))) * (molef-co)) + (21.725 * (ln (total-pressure / 101325)) * (axial-velocity / total-temperature))) * (molef-h2)) + (21.725 * (ln (total-pressure / 101325)) * (axial-velocity / total-temperature))) * (molef-co2))) + (((8.314 * 9.57 * 10 ^ (- 3)) * (axial-velocity / total-temperature) * (total-temperature - 273 - (273 * ln (total-temperature / 273))))) * (molef-ch4 * ((3.86 * (total-temperature - 273) - (((3.979 * 10 ^ (- 3)) / 2) * ((total-temperature ^ 2) - (273 ^ 2))) + (((24.558 * 10 ^ (- 6)) / 3) * ((total-temperature ^ 3) - (273 ^ 3))) - (((22.733 * 10 ^ (- 9)) / 4) * ((total-temperature ^ 4) - (273 ^ 4))) + (((6.963 * 10 ^ (- 12)) / 5) * ((total-temperature ^ 5) - (273 ^ 5))))))) + (((8.314 * 9.57 * 10 ^ (- 3)) * (axial-velocity / total-temperature) * (total-temperature - 273 - (273 * ln (total-temperature / 273))))) * (molef-h2o * ((4.07 * (total-temperature - 273)) - (((1.108 * 10 ^ (- 3)) / 2) * ((total-temperature ^ 2) - (273 ^ 2))) + (((4.152 * 10 ^ (- 6)) / 3) * ((total-temperature ^ 3) - (273 ^ 3))) - (((2.964 * 10 ^ (- 9)) / 4) * ((total-temperature ^ 4) - (273 ^ 4))) + (((0.807 * 10 ^ (- 12)) / 5) * ((total-temperature ^ 5) - (273 ^ 5)))))) + (((8.314 * 9.57 * 10 ^ (- 3)) * (axial-velocity / total-temperature) * (total-temperature - 273 - (273 * ln (total-temperature / 273))))) * (molef-co * ((3.71 * (total-temperature - 273)) - (((1.619 * 10 ^ (- 3)) / 2) * ((total-temperature ^ 2) - (273 ^ 2))) + (((3.692 * 10 ^ (- 6)) / 3) * ((total-temperature ^ 3) - (273 ^ 3))) - (((2.032 * 10 ^ (- 9)) / 4) * ((total-temperature ^ 4) - (273 ^ 4))) + (((0.24 * 10 ^ (- 12)) / 5) * ((total-temperature ^ 5) - (273 ^ 5)))))) + (((8.314 * 9.57 * 10 ^ (- 3)) * (axial-velocity / total-temperature) * (total-temperature - 273 - (273 * ln (total-temperature / 273))))) * (molef-h2 * ((3.057 * (total-temperature - 273)) + (((2.677 * 10 ^ (- 3)) / 2) * ((total-temperature ^ 2) - (273 ^ 2))) - (((5.81 * 10 ^ (- 6)) / 3) * ((total-temperature ^ 3) - (273 ^ 3))) + (((5.521 * 10 ^ (- 9)) / 4) * ((total-temperature ^ 4) - (273 ^ 4))) - (((1.812 * 10 ^ (- 12)) / 5) * ((total-temperature ^ 5) -

(273 ^ 5)))))) **+ (**((8.314 * 9.57 * 10 ^ (- 3)) * (axial-velocity / total-temperature) * (total-temperature - 273 - (273 * ln (total-temperature / 273)))) ***** (molef-co2 * ((2.401 * (total-temperature - 273)) + (((8.735 * 10 ^ (- 3)) / 2) * ((total-temperature ^ 2) - (273 ^ 2))) - (((6.607 * 10 ^ (- 6)) / 3) * ((total-temperature ^ 3) - (273 ^ 3))) + (((2 * 10 ^ (- 9)) / 4) * ((total-temperature ^ 4) - (273 ^ 4)))))) **)**

Total chemical exergy = ((- 50790 * (=(9.57 * 10 ^ (- 3) * (axial-velocity / total-temperature))) * molef-ch4)) + ((21.725 * (ln (total-pressure / 101325)) * (axial-velocity / total-temperature)) * (molef-ch4)) + ((8.314 * 9.57 * 10 ^ (- 3)) * (axial-velocity / total-temperature) * (total-temperature - 273 - (273 * ln (total-temperature / 273))))* (molef-ch4 * ((3.86 * (total-temperature - 273) - (((3.979 * 10 ^ (- 3)) / 2) * ((total-temperature ^ 2) - (273 ^ 2))) + (((24.558 * 10 ^ (- 6)) / 3) * ((total-temperature ^ 3) - (273 ^ 3))) - (((22.733 * 10 ^ (- 9)) / 4) * ((total-temperature ^ 4) - (273 ^ 4))) + (((6.963 * 10 ^ (- 12)) / 5) * ((total-temperature ^ 5) - (273 ^ 5)))))))+ (- 228590 * ((9.57 * 10 ^ (- 3) * (axial-velocity / total-temperature)) * molef-h2o) + ((21.725 * (ln (total-pressure / 101325)) * (axial-velocity / total-temperature)) * (molef-h2o)) + (((8.314 * 9.57 * 10 ^ (- 3)) * (axial-velocity / total-temperature) * (total-temperature - 273 - (273 * ln (total-temperature / 273)))) *(molef-h2o * ((4.07 * (total-temperature - 273)) - (((1.108 * 10 ^ (- 3)) / 2) * ((total-temperature ^ 2) - (273 ^ 2))) + (((4.152 * 10 ^ (- 6)) / 3) * ((total-temperature ^ 3) - (273 ^ 3))) - (((2.964 * 10 ^ (- 9)) / 4) * ((total-temperature ^ 4) - (273 ^ 4))) + (((0.807 * 10 ^ (- 12)) / 5) * ((total-temperature ^ 5) - (273 ^ 5)))))))) **-** (- 137150 * ((9.57 * 10 ^ (- 3) * (axial-velocity / total-temperature)) * molef-co)) + ((21.725 * (ln (total-pressure / 101325)) * (axial-velocity / total-temperature))) * (molef-co)) + (((8.314 * 9.57 * 10 ^ (- 3)) * (axial-velocity / total-temperature) * (total-temperature - 273 - (273 * ln (total-temperature / 273)))) * (molef-co * ((3.71 * (total-temperature - 273)) - (((1.619 * 10 ^ (- 3)) / 2) * ((total-temperature ^ 2) - (273 ^ 2))) + (((3.692 * 10 ^ (- 6)) / 3) * ((total-temperature ^ 3) - (273 ^ 3))) - (((2.032 * 10 ^ (- 9)) / 4) * ((total-temperature ^ 4) - (273 ^ 4))) + (((0.24 * 10 ^ (- 12)) / 5) * ((total-temperature ^ 5) - (273 ^ 5)))))) - (3 ***** ((21.725 * (ln (total-pressure / 101325)) * (axial-velocity / total-temperature))) * (molef-h2))+ (((8.314 * 9.57 * 10 ^ (- 3)) * (axial-velocity / total-temperature) * (total-temperature - 273 - (273 * ln (total-temperature / 273)))) * (molef-h2 * ((3.057 * (total-temperature - 273)) + (((2.677 * 10 ^ (- 3)) / 2) * ((total-temperature ^ 2) - (273 ^ 2))) - (((5.81 * 10 ^ (- 6)) / 3) * ((total-temperature

^ 3) - (273 ^ 3))) + (((5.521 * 10 ^ (- 9)) / 4) * ((total-temperature ^ 4) - (273 ^ 4))) - (((1.812 * 10 ^ (- 12)) / 5) * ((total-temperature ^ 5) - (273 ^ 5))))))) + ((- 50790 * (=(9.57 * 10 ^ (- 3) * (axial-velocity / total-temperature))) * molef-ch4)) + ((21.725 * (ln (total-pressure / 101325)) * (axial-velocity / total-temperature)) * (molef-ch4)) + ((8.314 * 9.57 * 10 ^ (- 3)) * (axial-velocity / total-temperature) * (total-temperature - 273 - (273 * ln (total-temperature / 273))))* (molef-ch4 * ((3.86 * (total-temperature - 273) - (((3.979 * 10 ^ (- 3)) / 2) * ((total-temperature ^ 2) - (273 ^ 2))) + (((24.558 * 10 ^ (- 6)) / 3) * ((total-temperature ^ 3) - (273 ^ 3))) - (((22.733 * 10 ^ (- 9)) / 4) * ((total-temperature ^ 4) - (273 ^ 4))) + (((6.963 * 10 ^ (- 12)) / 5) * ((total-temperature ^ 5) - (273 ^ 5))))))) + (2 * (- 228590 * ((9.57 * 10 ^ (- 3) * (axial-velocity / total-temperature)) * molef-h2o) + ((21.725 * (ln (total-pressure / 101325)) * (axial-velocity / total-temperature)) * (molef-h2o)) + (((8.314 * 9.57 * 10 ^ (- 3)) * (axial-velocity / total-temperature) * (total-temperature - 273 - (273 * ln (total-temperature / 273)))) *(molef-h2o * ((4.07 * (total-temperature - 273)) - (((1.108 * 10 ^ (- 3)) / 2) * ((total-temperature ^ 2) - (273 ^ 2))) + (((4.152 * 10 ^ (- 6)) / 3) * ((total-temperature ^ 3) - (273 ^ 3))) - (((2.964 * 10 ^ (- 9)) / 4) * ((total-temperature ^ 4) - (273 ^ 4))) + (((0.807 * 10 ^ (- 12)) / 5) * ((total-temperature ^ 5) - (273 ^ 5)))))))) - (- 394380 * ((9.57 * 10 ^ (- 3) * (axial-velocity / total-temperature)) * molef-co2)) + ((21.725 * (ln (total-pressure / 101325)) * (axial-velocity / total-temperature))) * (molef-co2) + (((8.314 * 9.57 * 10 ^ (- 3)) * (axial-velocity / total-temperature) * (total-temperature - 273 - (273 * ln (total-temperature / 273)))) * (molef-co2 * ((2.401 * (total-temperature - 273)) + (((8.735 * 10 ^ (- 3)) / 2) * ((total-temperature ^ 2) - (273 ^ 2))) - (((6.607 * 10 ^ (- 6)) / 3) * ((total-temperature ^ 3) - (273 ^ 3))) + (((2 * 10 ^ (- 9)) / 4) * ((total-temperature ^ 4) - (273 ^ 4))))))) - (4 * ((21.725 * (ln (total-pressure / 101325)) * (axial-velocity / total-temperature))) * (molef-h2))+ (((8.314 * 9.57 * 10 ^ (- 3)) * (axial-velocity / total-temperature) * (total-temperature - 273 - (273 * ln (total-temperature / 273)))) * (molef-h2 * ((3.057 * (total-temperature - 273)) + (((2.677 * 10 ^ (- 3)) / 2) * ((total-temperature ^ 2) - (273 ^ 2))) - (((5.81 * 10 ^ (- 6)) / 3) * ((total-temperature ^ 3) - (273 ^ 3))) + (((5.521 * 10 ^ (- 9)) / 4) * ((total-temperature ^ 4) - (273 ^ 4))) - (((1.812 * 10 ^ (- 12)) / 5) * ((total-temperature ^ 5) - (273 ^ 5))))))) +((- 137150 * ((9.57 * 10 ^ (- 3) * (axial-velocity / total-temperature)) * molef-co)) + ((21.725 * (ln (total-pressure / 101325)) * (axial-velocity / total-temperature))) * (molef-co)) + (((8.314 * 9.57 * 10 ^ (- 3)) * (axial-velocity / total-temperature) * (total-

temperature - 273 - (273 * ln (total-temperature / 273)))) * (molef-co * ((3.71 * (total-temperature - 273)) - (((1.619 * 10 ^ (- 3)) / 2) * ((total-temperature ^ 2) - (273 ^ 2))) + (((3.692 * 10 ^ (- 6)) / 3) * ((total-temperature ^ 3) - (273 ^ 3))) - (((2.032 * 10 ^ (- 9)) / 4) * ((total-temperature ^ 4) - (273 ^ 4))) + (((0.24 * 10 ^ (- 12)) / 5) * ((total-temperature ^ 5) - (273 ^ 5))))))) + ((- 50790 * (=(9.57 * 10 ^ (- 3) * (axial-velocity / total-temperature))) * molef-ch4)) + ((21.725 * (ln (total-pressure / 101325)) * (axial-velocity / total-temperature)) * (molef-ch4)) + ((8.314 * 9.57 * 10 ^ (- 3)) * (axial-velocity / total-temperature) * (total-temperature - 273 - (273 * ln (total-temperature / 273)))))* (molef-ch4 * ((3.86 * (total-temperature - 273) - (((3.979 * 10 ^ (- 3)) / 2) * ((total-temperature ^ 2) - (273 ^ 2))) + (((24.558 * 10 ^ (- 6)) / 3) * ((total-temperature ^ 3) - (273 ^ 3))) - (((22.733 * 10 ^ (- 9)) / 4) * ((total-temperature ^ 4) - (273 ^ 4))) + (((6.963 * 10 ^ (- 12)) / 5) * ((total-temperature ^ 5) - (273 ^ 5))))))) - (- 394380 * ((9.57 * 10 ^ (- 3) * (axial-velocity / total-temperature)) * molef-co2)) + ((21.725 * (ln (total-pressure / 101325)) * (axial-velocity / total-temperature))) * (molef-co2) + (((8.314 * 9.57 * 10 ^ (- 3)) * (axial-velocity / total-temperature) * (total-temperature - 273 - (273 * ln (total-temperature / 273)))) * (molef-co2 * ((2.401 * (total-temperature - 273)) + (((8.735 * 10 ^ (- 3)) / 2) * ((total-temperature ^ 2) - (273 ^ 2))) - (((6.607 * 10 ^ (- 6)) / 3) * ((total-temperature ^ 3) - (273 ^ 3))) + (((2 * 10 ^ (- 9)) / 4) * ((total-temperature ^ 4) - (273 ^ 4))))))) - ((21.725 * (ln (total-pressure / 101325)) * (axial-velocity / total-temperature))) * (molef-h2))+ (((8.314 * 9.57 * 10 ^ (- 3)) * (axial-velocity / total-temperature) * (total-temperature - 273 - (273 * ln (total-temperature / 273)))) * (molef-h2 * ((3.057 * (total-temperature - 273)) + (((2.677 * 10 ^ (- 3)) / 2) * ((total-temperature ^ 2) - (273 ^ 2))) - (((5.81 * 10 ^ (- 6)) / 3) * ((total-temperature ^ 3) - (273 ^ 3))) + (((5.521 * 10 ^ (- 9)) / 4) * ((total-temperature ^ 4) - (273 ^ 4))) - (((1.812 * 10 ^ (- 12)) / 5) * ((total-temperature ^ 5) - (273 ^ 5)))))))

Mixing exergy = a + b + c1 + d + e ((21.725 * (ln (total-pressure / 101325)) * (axial-velocity / total-temperature)) * (molef-ch4)) + ((21.725 * (ln (total-pressure / 101325)) * (axial-velocity / total-temperature)) * (molef-h2o))+((21.725 * (ln (total-pressure / 101325)) * (axial-velocity / total-temperature))) * (molef-co))+((21.725 * (ln (total-pressure / 101325)) * (axial-velocity / total-temperature))) * (molef-h2))+((21.725 * (ln (total-pressure / 101325)) * (axial-velocity / total-temperature))) * (molef-co2)).

Total exergy = ((21.725 * (ln (total-pressure / 101325)) * (axial-velocity / total-temperature)) * (molef-ch4))+ (21.725 * (ln (total-pressure / 101325)) * (axial-velocity / total-temperature)) * (molef-h2o))+ (21.725 * (ln (total-pressure / 101325)) * (axial-velocity / total-temperature))) * (molef-co)) + (21.725 * (ln (total-pressure / 101325)) * (axial-velocity / total-temperature))) * (molef-h2)) + (21.725 * (ln (total-pressure / 101325)) * (axial-velocity / total-temperature))) * (molef-co2))**)** + **(**(((8.314 * 9.57 * 10 ^ (- 3)) * (axial-velocity / total-temperature) * (total-temperature - 273 - (273 * ln (total-temperature / 273)))))***** (molef-ch4 * ((3.86 * (total-temperature - 273) - (((3.979 * 10 ^ (- 3)) / 2) * ((total-temperature ^ 2) - (273 ^ 2))) + (((24.558 * 10 ^ (- 6)) / 3) * ((total-temperature ^ 3) - (273 ^ 3))) - (((22.733 * 10 ^ (- 9)) / 4) * ((total-temperature ^ 4) - (273 ^ 4))) + (((6.963 * 10 ^ (- 12)) / 5) * ((total-temperature ^ 5) - (273 ^ 5))))))) + **(**(((8.314 * 9.57 * 10 ^ (- 3)) * (axial-velocity / total-temperature) * (total-temperature - 273 - (273 * ln (total-temperature / 273))))) ***** (molef-h2o * ((4.07 * (total-temperature - 273)) - (((1.108 * 10 ^ (- 3)) / 2) * ((total-temperature ^ 2) - (273 ^ 2))) + (((4.152 * 10 ^ (- 6)) / 3) * ((total-temperature ^ 3) - (273 ^ 3))) - (((2.964 * 10 ^ (- 9)) / 4) * ((total-temperature ^ 4) - (273 ^ 4))) + (((0.807 * 10 ^ (- 12)) / 5) * ((total-temperature ^ 5) - (273 ^ 5)))))) + **(**(((8.314 * 9.57 * 10 ^ (- 3)) * (axial-velocity / total-temperature) * (total-temperature - 273 - (273 * ln (total-temperature / 273))))) ***** (molef-co * ((3.71 * (total-temperature - 273)) - (((1.619 * 10 ^ (- 3)) / 2) * ((total-temperature ^ 2) - (273 ^ 2))) + (((3.692 * 10 ^ (- 6)) / 3) * ((total-temperature ^ 3) - (273 ^ 3))) - (((2.032 * 10 ^ (- 9)) / 4) * ((total-temperature ^ 4) - (273 ^ 4))) + (((0.24 * 10 ^ (- 12)) / 5) * ((total-temperature ^ 5) - (273 ^ 5)))))) + **(**(((8.314 * 9.57 * 10 ^ (- 3)) * (axial-velocity / total-temperature) * (total-temperature - 273 - (273 * ln (total-temperature / 273))))) ***** (molef-h2 * ((3.057 * (total-temperature - 273)) + (((2.677 * 10 ^ (- 3)) / 2) * ((total-temperature ^ 2) - (273 ^ 2))) - (((5.81 * 10 ^ (- 6)) / 3) * ((total-temperature ^ 3) - (273 ^ 3))) + (((5.521 * 10 ^ (- 9)) / 4) * ((total-temperature ^ 4) - (273 ^ 4))) - (((1.812 * 10 ^ (- 12)) / 5) * ((total-temperature ^ 5) - (273 ^ 5)))))**)** + **(**(((8.314 * 9.57 * 10 ^ (- 3)) * (axial-velocity / total-temperature) * (total-temperature - 273 - (273 * ln (total-temperature / 273))))) ***** (molef-co2 * ((2.401 * (total-temperature - 273)) + (((8.735 * 10 ^ (- 3)) / 2) * ((total-temperature ^ 2) - (273 ^ 2))) - (((6.607 * 10 ^ (- 6)) / 3) * ((total-temperature ^ 3) - (273 ^ 3))) +

(((2 * 10 ^ (- 9)) / 4) * ((total-temperature ^ 4) - (273 ^ 4)))))) + (total chemical exergy) = ((- 50790 * (=(9.57 * 10 ^ (- 3) * (axial-velocity / total-temperature))) * molef-ch4)) + ((21.725 * (ln (total-pressure / 101325)) * (axial-velocity / total-temperature)) * (molef-ch4)) + ((8.314 * 9.57 * 10 ^ (- 3)) * (axial-velocity / total-temperature) * (total-temperature - 273 - (273 * ln (total-temperature / 273))))) * (molef-ch4 * ((3.86 * (total-temperature - 273) - (((3.979 * 10 ^ (- 3)) / 2) * ((total-temperature ^ 2) - (273 ^ 2))) + (((24.558 * 10 ^ (- 6)) / 3) * ((total-temperature ^ 3) - (273 ^ 3))) - (((22.733 * 10 ^ (- 9)) / 4) * ((total-temperature ^ 4) - (273 ^ 4))) + (((6.963 * 10 ^ (- 12)) / 5) * ((total-temperature ^ 5) - (273 ^ 5)))))))+ (- 228590 * ((9.57 * 10 ^ (- 3) * (axial-velocity / total-temperature)) * molef-h2o) + ((21.725 * (ln (total-pressure / 101325)) * (axial-velocity / total-temperature)) * (molef-h2o)) + (((8.314 * 9.57 * 10 ^ (- 3)) * (axial-velocity / total-temperature) * (total-temperature - 273 - (273 * ln (total-temperature / 273)))) *(molef-h2o * ((4.07 * (total-temperature - 273)) - (((1.108 * 10 ^ (- 3)) / 2) * ((total-temperature ^ 2) - (273 ^ 2))) + (((4.152 * 10 ^ (- 6)) / 3) * ((total-temperature ^ 3) - (273 ^ 3))) - (((2.964 * 10 ^ (- 9)) / 4) * ((total-temperature ^ 4) - (273 ^ 4))) + (((0.807 * 10 ^ (- 12)) / 5) * ((total-temperature ^ 5) - (273 ^ 5)))))))) - (- 137150 * ((9.57 * 10 ^ (- 3) * (axial-velocity / total-temperature)) * molef-co)) + ((21.725 * (ln (total-pressure / 101325)) * (axial-velocity / total-temperature))) * (molef-co)) + (((8.314 * 9.57 * 10 ^ (- 3)) * (axial-velocity / total-temperature) * (total-temperature - 273 - (273 * ln (total-temperature / 273)))) * (molef-co * ((3.71 * (total-temperature - 273)) - (((1.619 * 10 ^ (- 3)) / 2) * ((total-temperature ^ 2) - (273 ^ 2))) + (((3.692 * 10 ^ (- 6)) / 3) * ((total-temperature ^ 3) - (273 ^ 3))) - (((2.032 * 10 ^ (- 9)) / 4) * ((total-temperature ^ 4) - (273 ^ 4))) + (((0.24 * 10 ^ (- 12)) / 5) * ((total-temperature ^ 5) - (273 ^ 5)))))) - (3 * ((21.725 * (ln (total-pressure / 101325)) * (axial-velocity / total-temperature))) * (molef-h2))+ (((8.314 * 9.57 * 10 ^ (- 3)) * (axial-velocity / total-temperature) * (total-temperature - 273 - (273 * ln (total-temperature / 273)))) * (molef-h2 * ((3.057 * (total-temperature - 273)) + (((2.677 * 10 ^ (- 3)) / 2) * ((total-temperature ^ 2) - (273 ^ 2))) - (((5.81 * 10 ^ (- 6)) / 3) * ((total-temperature ^ 3) - (273 ^ 3))) + (((5.521 * 10 ^ (- 9)) / 4) * ((total-temperature ^ 4) - (273 ^ 4))) - (((1.812 * 10 ^ (- 12)) / 5) * ((total-temperature ^ 5) - (273 ^ 5)))))) + ((- 50790 * (=(9.57 * 10 ^ (- 3) * (axial-velocity / total-temperature))) * molef-ch4)) + ((21.725 * (ln (total-pressure / 101325)) * (axial-velocity / total-temperature)) * (molef-ch4)) + ((8.314 * 9.57 * 10 ^ (- 3)) * (axial-velocity / total-temperature) * (total-

temperature - 273 - (273 * ln (total-temperature / 273)))))* (molef-ch4 * ((3.86 * (total-temperature - 273) - (((3.979 * 10 ^ (- 3)) / 2) * ((total-temperature ^ 2) - (273 ^ 2))) + (((24.558 * 10 ^ (- 6)) / 3) * ((total-temperature ^ 3) - (273 ^ 3))) - (((22.733 * 10 ^ (- 9)) / 4) * ((total-temperature ^ 4) - (273 ^ 4))) + (((6.963 * 10 ^ (- 12)) / 5) * ((total-temperature ^ 5) - (273 ^ 5))))))) + (2 * (- 228590 * ((9.57 * 10 ^ (- 3) * (axial-velocity / total-temperature)) * molef-h2o) + ((21.725 * (ln (total-pressure / 101325)) * (axial-velocity / total-temperature)) * (molef-h2o)) + (((8.314 * 9.57 * 10 ^ (- 3)) * (axial-velocity / total-temperature) * (total-temperature - 273 - (273 * ln (total-temperature / 273)))) *(molef-h2o * ((4.07 * (total-temperature - 273)) - (((1.108 * 10 ^ (- 3)) / 2) * ((total-temperature ^ 2) - (273 ^ 2))) + (((4.152 * 10 ^ (- 6)) / 3) * ((total-temperature ^ 3) - (273 ^ 3))) - (((2.964 * 10 ^ (- 9)) / 4) * ((total-temperature ^ 4) - (273 ^ 4))) + (((0.807 * 10 ^ (- 12)) / 5) * ((total-temperature ^ 5) - (273 ^ 5)))))))) - (- 394380 * ((9.57 * 10 ^ (- 3) * (axial-velocity / total-temperature)) * molef-co2)) + ((21.725 * (ln (total-pressure / 101325)) * (axial-velocity / total-temperature))) * (molef-co2) + (((8.314 * 9.57 * 10 ^ (- 3)) * (axial-velocity / total-temperature) * (total-temperature - 273 - (273 * ln (total-temperature / 273)))) * (molef-co2 * ((2.401 * (total-temperature - 273)) + (((8.735 * 10 ^ (- 3)) / 2) * ((total-temperature ^ 2) - (273 ^ 2))) - (((6.607 * 10 ^ (- 6)) / 3) * ((total-temperature ^ 3) - (273 ^ 3))) + (((2 * 10 ^ (- 9)) / 4) * ((total-temperature ^ 4) - (273 ^ 4))))))) - (4 * ((21.725 * (ln (total-pressure / 101325)) * (axial-velocity / total-temperature))) * (molef-h2))+ (((8.314 * 9.57 * 10 ^ (- 3)) * (axial-velocity / total-temperature) * (total-temperature - 273 - (273 * ln (total-temperature / 273)))) * (molef-h2 * ((3.057 * (total-temperature - 273)) + (((2.677 * 10 ^ (- 3)) / 2) * ((total-temperature ^ 2) - (273 ^ 2))) - (((5.81 * 10 ^ (- 6)) / 3) * ((total-temperature ^ 3) - (273 ^ 3))) + (((5.521 * 10 ^ (- 9)) / 4) * ((total-temperature ^ 4) - (273 ^ 4))) - (((1.812 * 10 ^ (- 12)) / 5) * ((total-temperature ^ 5) - (273 ^ 5))))))).) +((- 137150 * ((9.57 * 10 ^ (- 3) * (axial-velocity / total-temperature)) * molef-co)) + ((21.725 * (ln (total-pressure / 101325)) * (axial-velocity / total-temperature))) * (molef-co)) + (((8.314 * 9.57 * 10 ^ (- 3)) * (axial-velocity / total-temperature) * (total-temperature - 273 - (273 * ln (total-temperature / 273)))) * (molef-co * ((3.71 * (total-temperature - 273)) - (((1.619 * 10 ^ (- 3)) / 2) * ((total-temperature ^ 2) - (273 ^ 2))) + (((3.692 * 10 ^ (- 6)) / 3) * ((total-temperature ^ 3) - (273 ^ 3))) - (((2.032 * 10 ^ (- 9)) / 4) * ((total-temperature ^ 4) - (273 ^ 4))) + (((0.24 * 10 ^ (- 12)) / 5) * ((total-temperature ^ 5) - (273 ^ 5))))))) + ((- 50790 * (=(9.57 * 10 ^ (- 3)

* (axial-velocity / total-temperature))) * molef-ch4)) + ((21.725 * (ln (total-pressure / 101325)) * (axial-velocity / total-temperature)) * (molef-ch4)) + ((8.314 * 9.57 * 10 ^ (- 3)) * (axial-velocity / total-temperature) * (total-temperature - 273 - (273 * ln (total-temperature / 273)))))* (molef-ch4 * ((3.86 * (total-temperature - 273) - (((3.979 * 10 ^ (- 3)) / 2) * ((total-temperature ^ 2) - (273 ^ 2))) + (((24.558 * 10 ^ (- 6)) / 3) * ((total-temperature ^ 3) - (273 ^ 3))) - (((22.733 * 10 ^ (- 9)) / 4) * ((total-temperature ^ 4) - (273 ^ 4))) + (((6.963 * 10 ^ (- 12)) / 5) * ((total-temperature ^ 5) - (273 ^ 5))))))) - (- 394380 * ((9.57 * 10 ^ (- 3) * (axial-velocity / total-temperature)) * molef-co2)) + ((21.725 * (ln (total-pressure / 101325)) * (axial-velocity / total-temperature))) * (molef-co2) + (((8.314 * 9.57 * 10 ^ (- 3)) * (axial-velocity / total-temperature) * (total-temperature - 273 - (273 * ln (total-temperature / 273)))) * (molef-co2 * ((2.401 * (total-temperature - 273)) + (((8.735 * 10 ^ (- 3)) / 2) * ((total-temperature ^ 2) - (273 ^ 2))) - (((6.607 * 10 ^ (- 6)) / 3) * ((total-temperature ^ 3) - (273 ^ 3))) + (((2 * 10 ^ (- 9)) / 4) * ((total-temperature ^ 4) - (273 ^ 4))))))) - ((21.725 * (ln (total-pressure / 101325)) * (axial-velocity / total-temperature))) * (molef-h2))+ (((8.314 * 9.57 * 10 ^ (- 3)) * (axial-velocity / total-temperature) * (total-temperature - 273 - (273 * ln (total-temperature / 273)))) * (molef-h2 * ((3.057 * (total-temperature - 273)) + (((2.677 * 10 ^ (- 3)) / 2) * ((total-temperature ^ 2) - (273 ^ 2))) - (((5.81 * 10 ^ (- 6)) / 3) * ((total-temperature ^ 3) - (273 ^ 3))) + (((5.521 * 10 ^ (- 9)) / 4) * ((total-temperature ^ 4) - (273 ^ 4))) - (((1.812 * 10 ^ (- 12)) / 5) * ((total-temperature ^ 5) - (273 ^ 5))))))) + ((21.725 * (ln (total-pressure / 101325)) * (axial-velocity / total-temperature)) * (molef-ch4)) + ((21.725 * (ln (total-pressure / 101325)) * (axial-velocity / total-temperature)) * (molef-h2o))+((21.725 * (ln (total-pressure / 101325)) * (axial-velocity / total-temperature))) * (molef-co))+((21.725 * (ln (total-pressure / 101325)) * (axial-velocity / total-temperature))) * (molef-h2))+((21.725 * (ln (total-pressure / 101325)) * (axial-velocity / total-temperature))) * (molef-co2)).

References

[1] Zhai, X., et al., *CFD simulation with detailed chemistry of steam reforming of methane for hydrogen production in an integrated micro-reactor.* International Journal of Hydrogen Energy, 2010. **35**(11): p. 5383-5392.

[2] Irani, M., et al., *CFD modeling of hydrogen production using steam reforming of methane in monolith reactors: Surface or volume-base reaction model?* International journal of hydrogen energy, 2011. **36**(24): p. 15602-15610.

[3] Saeidi, S., et al., *Hydrogen production: Perspectives, separation with special emphasis on kinetics of WGS reaction: A state-of-the-art review.* Journal of Industrial and Engineering Chemistry, 2017. **49**: p. 1-25.

[4] Baharudin, L. and M.J. Watson, *Monolithic substrate support catalyst design considerations for steam methane reforming operation.* Reviews in Chemical Engineering, 2018. **34**(4): p. 481-501.

[5] Tzanetis, K., C. Martavaltzi, and A. Lemonidou, *Comparative exergy analysis of sorption enhanced and conventional methane steam reforming.* international journal of hydrogen energy, 2012. **37**(21): p. 16308-16320.

[6] Simpson, A.P. and A.E. Lutz, *Exergy analysis of hydrogen production via steam methane reforming.* International Journal of Hydrogen Energy, 2007. **32**(18): p. 4811-4820.

[7] Lao, L., et al., *CFD modeling and control of a steam methane reforming reactor.* Chemical Engineering Science, 2016. **148**: p. 78-92.

[8] Hajjaji, N., et al., *Exergy analysis: An efficient tool for understanding and improving hydrogen production via the steam methane reforming process.* Energy Policy, 2012. **42**: p. 392-399.

[9] Palma, V., et al., *Monolithic catalysts for methane steam reforming intensification: Experimental and numerical investigations.* Fuel, 2014. **138**: p. 80-90.

[10] Alabi, K. and F. Ladeinde. *Utilizing CFD-based exergy calculations in the design/optimization of a complete aircraft system*. in *45th AIAA Aerospace Sciences Meeting and Exhibit*. 2007.

[11] Karakaya, C., L. Maier, and O. Deutschmann, *Surface reaction kinetics of the oxidation and reforming of CH4 over Rh/Al2O3 catalysts.* International Journal of Chemical Kinetics, 2016. **48**(3): p. 144-160.

[12] Thormann, J., et al., *Steam reforming of hexadecane over a Rh/CeO2 catalyst in microchannels: Experimental and numerical investigation.* international journal of hydrogen energy, 2009. **34**(12): p. 5108-5120.

[13] Mundhwa, M. and C.P. Thurgood, *Numerical study of methane steam reforming and methane combustion over the segmented and continuously coated layers of catalysts in a plate reactor.* Fuel Processing Technology, 2017. **158**: p. 57-72.

[14] Deutschmann, O., et al., *Natural gas conversion in monolithic catalysts: interaction of chemical reactions and transport phenomena*, in *Studies in Surface Science and Catalysis*. 2001, Elsevier. p. 251-258.

[15] Deutschmann, O. and L.D. Schmidt. *Two-dimensional modeling of partial oxidation of methane on rhodium in a short contact time reactor*. in *Symposium (International) on Combustion*. 1998. Elsevier.

[16] Sato, N., *Chemical energy and exergy: an introduction to chemical thermodynamics for engineers*. 2004: Elsevier.

[17] Szargut, J., *Exergy method: technical and ecological applications*. Vol. 18. 2005: WIT press.

[18] Dincer, I. and M.A. Rosen, *Exergy: energy, environment and sustainable development*. 2012: Newnes.

[19] Mustafa, J., et al., *Computational fluid dynamics based model development and exergy analysis of naphtha reforming reactors.* International Journal of Exergy, 2017. **24**(2-4): p. 344-363.

[20] Moran, M.J., et al., *Fundamentals of engineering thermodynamics*. 2010: John Wiley & Sons.

[21] Hinderink, A., et al., *Exergy analysis with a flowsheeting simulator—I. Theory; calculating exergies of material streams.* Chemical Engineering Science, 1996. **51**(20): p. 4693-4700.

[22] Querol, E., B. Gonzalez-Regueral, and J.L. Perez-Benedito, *Exergy concept and determination*, in *Practical Approach to Exergy and Thermoeconomic Analyses of Industrial Processes*. 2013, Springer. p. 9-28.

[23] Farmahini–Farahani, M., *Investigation of four geometrical parameters on thermal stratification of cold water tanks by exergy analysis.* International Journal of Exergy, 2012. **10**(3): p. 332-345.

[24] Alabi, K. and F. Ladeinde. *Utilizing CFD-Based Exergy Calculations in the Design/Optimization of a Complete Aircraft System*. in *45th AIAA Aerospace Sciences Meeting and Exhibit*. 2007.

[25] Jafarmadar, S., *Exergy analysis of natural gas/diesel combustion in homogenous charge compression ignition engines (HCCI) using multi-dimensional model.* International Journal of Exergy, 2015. **17**(4): p. 475-491.

[26] Taylor, K., et al. *The prediction of pressure drop and flow distribution in packed bed filters*. in *Second International Conference on CFD in the Minerals and Process Industries, CSIRO*. 1999.

[27] Plascencia-Jatomea, R., et al., *Hydrodynamic study of a novel membrane aerated biofilm reactor (MABR): Tracer experiments and CFD simulation.* Chemical Engineering Science, 2015. **138**: p. 324-332.

[28] Boulenouar, M. and A. Ouadha. *CFD-Exergy analysis of the flow in a supersonic steam ejector*. in *Journal of Physics: Conference Series*. 2015. IOP Publishing.

[29] Alabi, K., et al. *A comparison of empirical and CFD-based exergy modelling for the airframe subsystem of aircraft design*. in *25th International congress of the aeronautical sciences*. 2006.

[30] Gunjo, D.G., P. Mahanta, and P.S. Robi, *Exergy and energy analysis of a novel type solar collector under steady state condition: Experimental and CFD analysis.* Renewable Energy, 2017. **114**: p. 655-669.

[31] Debnath, P. and K. Pandey, *Exergetic efficiency analysis of hydrogen–air detonation in pulse detonation combustor using computational fluid dynamics.* International Journal of Spray and Combustion Dynamics, 2017. **9**(1): p. 44-54.

[32] Erguvan, M. and D. MacPhee, *Energy and Exergy Analyses of Tube Banks in Waste Heat Recovery Applications.* Energies, 2018. **11**(8): p. 2094.

[33] Granlund, M.Z., et al., *Comparison between a micro reactor with multiple air inlets and a monolith reactor for oxidative steam reforming of diesel.* International journal of hydrogen energy, 2014. **39**(31): p. 18037-18045.

[34] Bhat, S.A. and J. Sadhukhan, *Process intensification aspects for steam methane reforming: an overview.* AIChE Journal, 2009. **55**(2): p. 408-422.

[35] Chen, J., et al., *Effect of heat and mass transfer on the combustion stability in catalytic micro-combustors.* Applied Thermal Engineering, 2018. **131**: p. 750-765.

[36] Yu, X., et al., *Development of a microchannel reactor concerning steam reforming of methanol.* Chemical Engineering Journal, 2006. **116**(2): p. 123-132.

[37] Theampetch, A., et al., *Design of Microreactor Flow Channel for Fischer Tropsch Synthesis Using Computational Fluid Dynamic.* Energy Procedia, 2016. **100**: p. 439-447.

[38] Kansha, Y., et al., *Evaluation of a self-heat recuperative thermal process based on thermodynamic irreversibility and exergy.* Journal of chemical engineering of Japan, 2012: p. 12we084.

[39] Hosseini, S.E. and M.A. Wahid, *Enhancement of exergy efficiency in combustion systems using flameless mode.* Energy conversion and management, 2014. **86**: p. 1154-1163.

[40] An, H., et al., *Computational fluid dynamics (CFD) analysis of micro-reactor performance: Effect of various configurations.* Chemical engineering science, 2012. **75**: p. 85-95.

[41] Kashid, M.N., D.W. Agar, and S. Turek, *CFD modelling of mass transfer with and without chemical reaction in the liquid–liquid slug flow microreactor.* Chemical Engineering Science, 2007. **62**(18-20): p. 5102-5109.

[42] Querol, E., B. Gonzalez-Regueral, and J.L. Perez-Benedito, *Practical approach to exergy and thermoeconomic analyses of industrial processes*. 2012: Springer Science & Business Media.

[43] Montelongo-Luna, J.M., W.Y. Svrcek, and B.R. Young, *The relative exergy array—a new measure for interactions in process design and control.* The Canadian Journal of Chemical Engineering, 2011. **89**(3): p. 545-549.

[44] Munir, M., W. Yu, and B. Young, *The relative exergy-destroyed array: A new tool for control structure design.* The Canadian Journal of Chemical Engineering, 2013. **91**(10): p. 1686-1694.

[45] Bahmanpour, A.M., A. Hoadley, and A. Tanksale, *Critical review and exergy analysis of formaldehyde production processes.* Reviews in Chemical Engineering, 2014. **30**(6): p. 583-604.

[46] Yong-an, A., et al. *Exergy analysis of exhaust-gas of burning liquefied-gas in a Chinese kitchen*. in *2009 International Conference on Energy and Environment Technology*. 2009. IEEE.

[47] Huang, X., et al., *Exergy distribution characteristics of solar-thermal dissociation of NiFe 2 O 4 in a solar reactor.* Energy, 2017. **123**: p. 131-138.

[48] Huang, X., et al., *Exergy distribution characteristics of solar-thermal dissociation of NiFe2O4 in a solar reactor.* Energy, 2017. **123**: p. 131-138.

[49] Cao, C., et al., *A comparative study of Rh and Ni coated microchannel reactor for steam methane reforming using CFD with detailed chemistry.* Chemical Engineering Science, 2015. **137**: p. 276-286.

[50] Versteeg, H.K. and W. Malalasekera, *An introduction to computational fluid dynamics: the finite volume method*. 2007: Pearson Education.

[51] Menon, K.G. and V.S. Patnaikuni, *CFD simulation of fuel reactor for chemical looping combustion of Indian coal.* Fuel, 2017. **203**: p. 90-101.